TECHNISCHE UNIVERSITÄT KAISERSLAUTERN

KIMA
Lehrstuhl für Konstruktion im Maschinen- und Apparatebau

MASTER THESIS

Title: **Multi-Body modelling of a Multi-Articulation-Tramway in SIMPACK v9 and Research into the Influence of Rail-Excitations on Forces acting in the Yaw Dampers**

Editors: Margarita Mármol Fernández

Adviser: Dipl.-Ing. Tobias Bettinger

Kaiserslautern, October 28, 2014

Master Thesis-Nr.:816

Project Definition

Statement

I, Margarita Mármol Fernández Matr. Nr. 391498

Declare that I have done this work by myself and without any help apart from the documents listed on the text and bibliography.

Kaiserslautern, 28 October 2014

Signature

Table of contents

List of Figures

List of Tables

List of Abbreviations

z_l	m	Virtual deviation for the left rail
x	m	Longitudinal direction
z_r	m	Virtual deviation for the right rail
y_l	m	Lateral deviation for the left rail
y_r	m	Virtual deviation for the right rail
h	m	Longitudinal height
u	m	Way position
s	m	Gauge
Ψ	m	Transverse position
f	Hz	Frequency
ω	rad/s	Angular frequency
T	s	Period
v	m/s	Velocity
t	s	Time
λ	m	Wavelength
k	1/m	Angular wavenumber
Δk	1/m	Wavenumber spectrum
b	m	Amplitude
ε	rad	Phase Angle
σ^2_h	mm^2	Variance
Φ_{hi}	$\frac{mm^2}{1/m}$	Power Unevenness Density
RFC	-	Rainflow Cycle Counting
S		Stress
RFM	-	Rainflow Matrix
RES	-	Residual
PSD	-	Power Spectral Density
FFT	-	Fast Fourier Transform
IFT	-	Inverse Fourier Transform

1 Introduction

The topic of this work is the study of the different fatigue damage appearing in a Combino SIEMENS tramway when running under different railway excitations. This is done by the study of the cycles counted in the yaw damper forces existing on it by applying the Rainflow Cycle Counting load analysis method.

A study of the dynamic behavior of a vehicle is needed to define its final design. Analyze these scenarios in a real prototype of the vehicle always supposes high investment. To solve this problem a Mulit-body Simulation Software is always used to simulate and analyze several scenarios before create the prototype. The main advantage of the creation of this model, beside the reduction of cost, is that it can be used to simulate different scenarios and study its behavior under different environments. The creation of this model using the Mulit-body Simulation Software and the afterwards study of some scenarios is the main goal of this work.

The work is divided into three big sections beside this Introduction.

Section 2 introduces some basic theoretical concepts needed to understand better the study. A big topic here explained is rail excitations, the reason of them, the way to study them, etc. The composition of the tramway under study, Combino SIEMENS, is also described here, as well as general tramway concepts.

One part with a big importance on this work is the load analysis. Several methods to analyze loads and obtain the cycles of them are explained and compared between them in this section. The main method described and also used afterwards for this study is the Rainflow Cycle Counting and the posteriori representation of the Rainflow Matrix. These concepts here explained are synthetized to create the Matlab function used in next sections to obtain the cycles of the forces/loads affecting in the fatigue damage.

The extraction of the forces to analyze is done in different simulation scenarios generated within a Combino tramway model design in Simpack v.9. The description of the model, a brief description of the software used (Simpack v.9 and Matlab) and the simulation scenarios under study are all explained in Section 3.

Once the forces are obtained in Simpack and the Rainflow Matrix related to them extracted in Matlab, the analysis of the results can be done.

2 Theoretical Foundations

2.1 Structure/composition of rolling stock

Wheels, axles and the attachment between them are the most critical parts of the railway rolling stock. A minimum fail on their design can cause derailment. The main characteristics of them will be following explained.

2.1.1 Wheel profiles

Rail wheels consist of four major elements: the flange, the hub, the disc and the tire, as shown in Figure 2.1. The main characteristic of a rail wheel is its conical shape, to enable track guiding. [1, pp. 46-47]

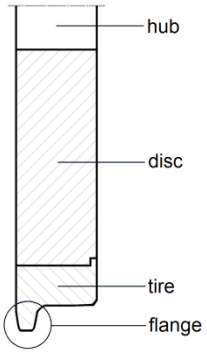

Figure 2.1: Wheel structure [2]

2.1.2 Rail profiles

The main type of rail is the well-known *Head-rail*. It consists of three parts: head, web and foot. Flat bottomed rail is the dominant head-rail profile and it is in worldwide use.
For tramways, because of the need of a rail laid in the pavement, a Grooved Rail is used. It is characterized by having a gap for the flange. Both rail-profiles are shown in Figure 2.2. [2]

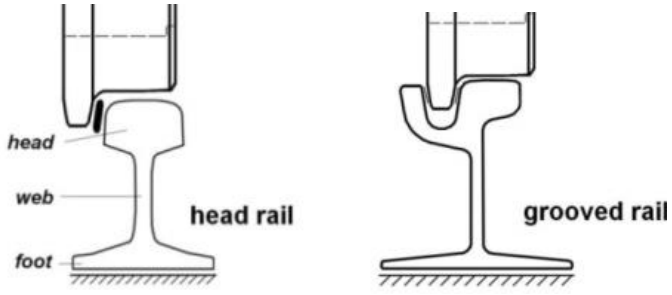

Figure 2.2: Head and grooved rail designs [2]

2.1.3 Track Guiding Principles

The main parts of a propulsion system are a traction motor, a gearbox and two wheelsheets. To achieve the need of reducing wheel-rail interaction forces by reducing the unsprung mass, the system is getting more complex.

The main different that can be found on the bogie configuration is regarding the weelset. The simplest is the transverse wheelset (Figure 2.3.a), where the wheels are coupled in the lateral direction via a fixed axle. More complex design are longitudinal wheelset, where the wheels are coupled in the lateral direction (Figure 2.3.b), and independent wheels, where there is not coupling between them (Figure 2.3.c). On the longitudinal wheelset configuration, the wheels are directly powered by the motor with a gearbox in between. Two motors are used, one on each side, powering at the same time the two wheels of their side. This space saving arrangement is especially suitable for 100% low-floor tramways. [3]

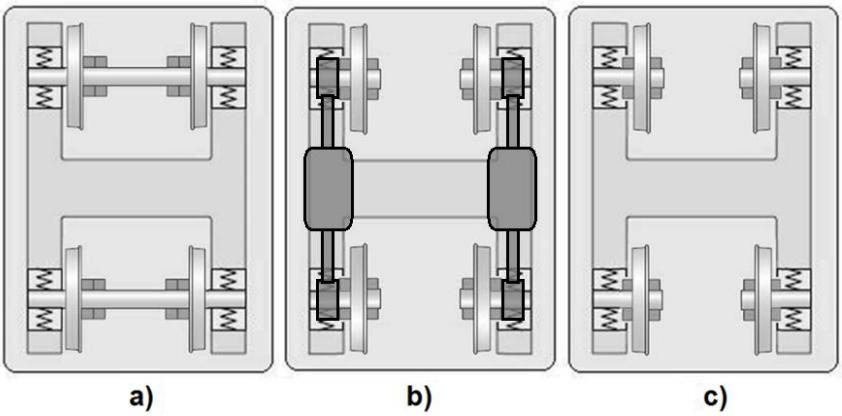

Figure 2.3: Transverse wheelset (a), Independent wheels (b) and Longitudinal wheelset (c) configurations. D.t. [3]

2.2 Railway Vehicles Dynamics

According to the dynamic properties of the wheel and rail, the roughness on their surface induces vertical vibration of the wheel and rail systems because of the interaction at their contact area. This vibration is transmitted into the wheel and track structures and afterwards, to the main vehicle. Figure 2.4 shows the rolling noise caused by wheel and rail vibrations induced at the wheel/rail contact. [4, pp. 6-7]

For that reason, in the railway system design, the study of the wheel-rail-contact dynamics is very important. This is done via wheel-rail contact dynamic models, which allow the study of the relation between the vibrations produced in a rail point, and the wheel-profile irregularities. [4, pp. 6-7]

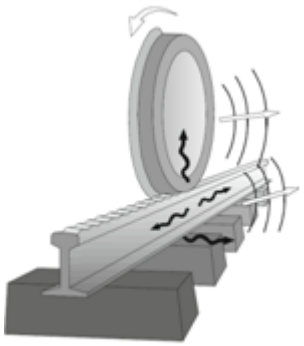

Figure 2.4: Rolling noise generation.Mechanism illustration [4, p. 7]

2.2.1 Contact Forces

The interface between the wheel and the rail is a small horizontal contact surface. Because of the small dimension of this area, the contact pressure on it is close to a stress concentration. The knowledge of these contact forces is necessary to determine the general wheelset equilibrium and its dynamic behavior. In the simplest model, only vertical contact forces are considered, but in the practice there are more contact forces taking place. This is because, though the roughness is acting in the vertical direction, the coupling between wheel and rail is also in lateral and longitudinal directions. When entering a curve or running on a track with irregularities (real track), the suspension forces create reaction forces at the wheel-rail contact area because of the strong link that these suspension elements create between the wheel and the main vehicle. [1, pp. 88-97] [4, p. 134] [5]

It is noteworthy, that on this study, the reference coordinate system is referred to a local axis system x´y´z´; where z´ is normal to the contact, y´ is relative to the transverse direction and x´ is along the track. According to this contact coordinate system, the contact forces are denoted as: N for normal forces, F_x for longitudinal creep force and F_y for lateral creep force. The name of the tangent components (lateral and longitudinal) is because of their relation to the relative speed between the two bodies in contact, called creepage. Figure 2.5 shows the reference coordinate system (in red), and the contact forces associated to it. [1, pp. 87-88]

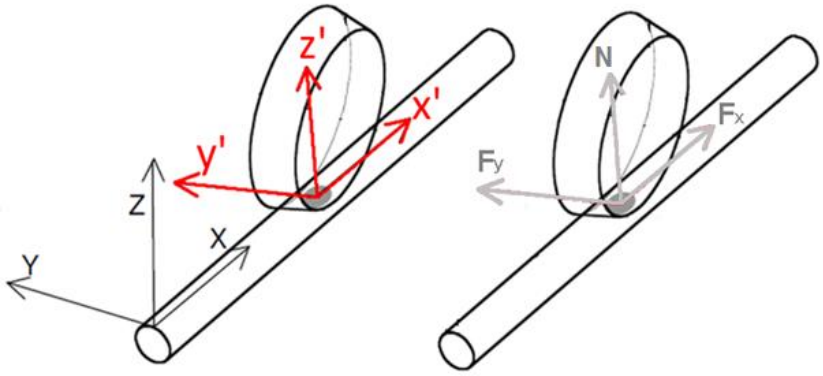

Figure 2.5: Contact coordinate system (left) and contact forces referred to it (right) [1, p 88]

2.2.2 Wheel-Rail-Contact.

Nowadays, the Wheel-Rail-Contact dynamic can be modelled by specific based on multi-body-systems dynamics programs. Those are grounded on the Classic Models, which determined these contact parameters in two steps: the vertical contact is analyzed via the non-lineal theory of Hertz, while Kalker's theory is used to idealize the tangential and longitudinal problem. Beside the vertical problem, tangential problem is the most important to study. [1, pp. 88-97] [4, p. 134] [5]

The Hertz theory is based on some hypothesis according to the wheel-rail contact: the behaviour of the two bodies in contact is elastic; the elliptical shape of the wheel can be neglected, that is, that the curvature radius is considered much bigger than the dimensions of the elliptic contact area; and the curvatures within the contact area are constant. With these hypotheses, the case under study is simplified to an ellipse-flatted contact surface, affected by a semi-ellipsoid contact pressure. Under these considerations, the Hertz theory obtains the vertical force F_x relating the vertical displacement of the wheel with its roughness profile and the vertical displacement of the

rail, via a non-lineal elastic spring of constant K_H. Figure 2.6 represents the two dynamic systems, wheel and rail, connected via a force element, K_H.

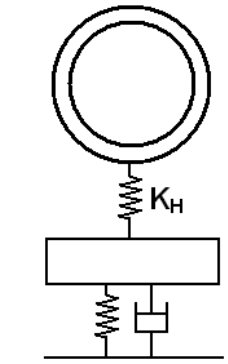

Figure 2.6: System characterization for the study of the vertical problem. D.t. [1, p. 88]

The most common used model for the tangent problem is the theory of Kalker. It establishes general expressions to determine these contact forces by introducing variable stiffness coefficients depending on the contact area of each case. This approximation gives coherent results for cases with a very small wheel creep. [1, pp. 88-97] [4, p. 134] [5]

2.2.3 Theoretical track game

The so called theoretical track game (σ) is the relation between the distance between rails (S) and the distance between wheels (s), see Figure 2.7:

$$\sigma = S - s \tag{2.1}$$

It represents the game existing between the wheels and the rails. As both distances are constant, the game is also a constant, which usually takes the value 10mm for tramways. This value will be used in Section 3.4 for the representation of lateral displacement of wheels and track. [1, pp.109-110]

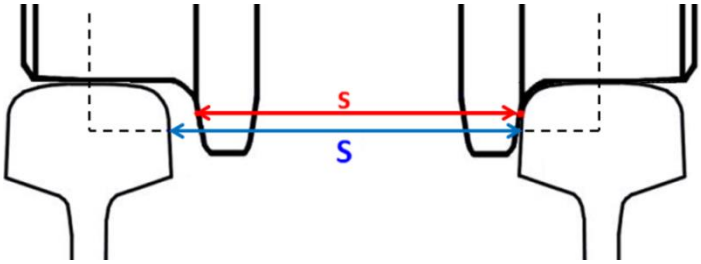

Figure 2.7: Representation of the distance between rails (S) and between wheels (s).D.t.[1, p.109]

2.3 Rail Excitations

When a train is running over a track, the real track is not ideal. This real track, with random shape compound of a sum of multiple sinus and cosines shapes, affects the above-travelling vehicle vibration system as an excitation.
The riding quality, equally dependent on the track geometry and on the dynamic characteristics of the vehicle, is then affected by this behavior. For that reason, these two parameters have to be deeply studied. [6]

The geometry of the track is well-done determined by the spatial position of the running rails, described, on its part, with the virtual deviation z and the lateral deviation y from a virtual straight. The four parameters ($z_l(x)$, $y_l(x)$ for the left rail, and $z_r(x)$, $y_r(x)$, for the right rail) specify the position of the rail along the explicit distance x, as shown in Figure 2.8.

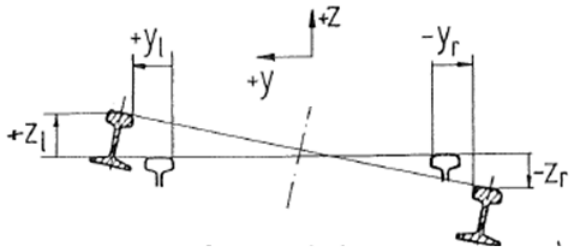

Figure 2.8: Rail position coordinates [6]

The spatial arrangement of the rails is also obtained referred to the track axle. It is defined by four parameters: longitudinal height h(x) and directional position u(x) of the track axle, plus the gauge s(x) and the transverse position Ψ(x), both running-rail correlated. All are together collected as the generic term *Track-Position* and are usually used in the engineering of the rail, see Figure 2.9. With these parameters, the coordinated system of the position is defined as:

$$z_l(x) = h(x) + \frac{s(x)}{2} sin\Psi(x), \qquad z_r(x) = h(x) - \frac{s(x)}{2} sin\Psi(x), \qquad \text{with} \qquad h(x) = \frac{z_l(x) + z_r(x)}{2}, \quad u(x) = \frac{y(x) + y_r(x)}{2}, \quad s(x) = s_0 + (y_l(x) - y_r(x)), \quad \Psi(x) = arctg \frac{z_l(x) - z_r(x)}{s_0 + (y(x) - y_r(x))} \tag{2.2}$$

$$y_l(x) = u(x) + \frac{s(x) - s_0}{2}, \qquad y_r(x) = u(x) - \frac{s(x) - s_0}{2},$$

s_0 = gauge in the position s_0.

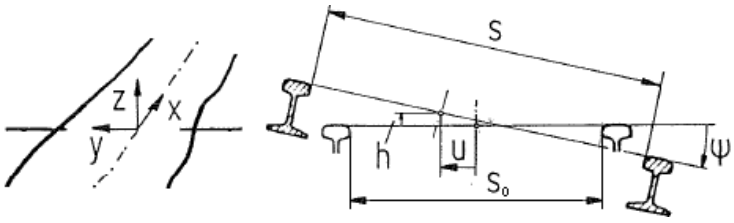

Figure 2.9: Track position coordinates [6]

The deviation of the actual position of the track for an allowed position is called T*rack-Position-Error*, which is the collection of the values up mentioned compared with its related nominal value. [6]

The vehicle responds to an absolute value of the *Track-Position* (h(x), u(x), s(x) and Ψ(x)). This value is affected by several factors: Irregularities in the rail slope and in the profile of the rail head, rail discontinuities and changes in the elastic characteristics of the rail. The sequence of disturbances in dependency of the road is well-known as *Disturbance Function*. [6]

2.3.1 Spectral Analysis

A sinusoidal track affects the above-travelling vehicle vibration system as an excitation. Driving with a car velocity v under a sinusoidal rail condition of wavelength λ, a frequency excitation of period

$$T = \lambda / v \tag{2.3}$$

appears, where its angular frequency associated is:

$$\omega = 2\pi \cdot f = 2\pi \cdot v/ \lambda. \tag{2.4}$$

For each parameter of the *Track-Position* belongs a frequency excitation in correlation with its wavelength associated, as shown in Figure 2.10. [6]

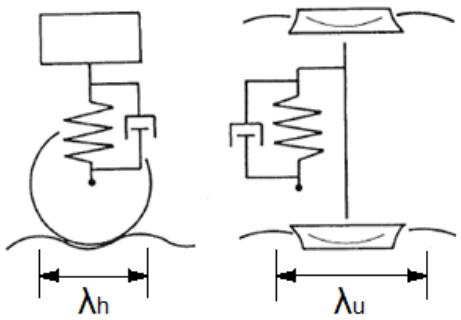

Figure 2.10: Rail position coordinates [6]

The correlation between the wavelength of the road λ, the velocity v and the frequency excitation f is showed in Figure 2.11 in double-logarithm representation. Excitations between 0,5 Hz and 20 Hz affect the vehicle comfort, while over 20 Hz can induced noise disturbance. [6]

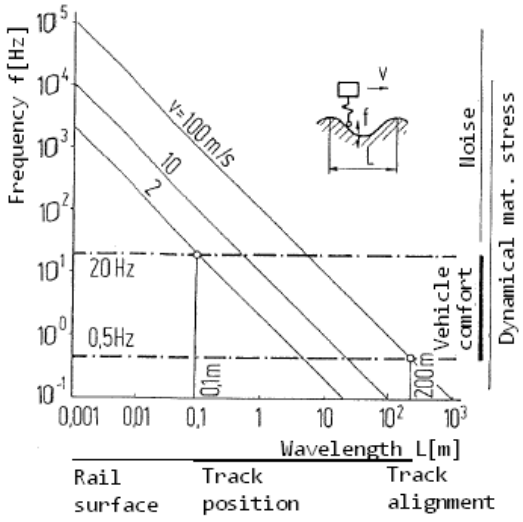

Figure 2.11: Correlation between wave lengths of the road L, velocity v and frequency excitation f, in double-logarithm representation [6]

In the actual *Track-Position* there is not only one wave length to determine, in fact, there are simultaneously numerous wavelengths, existing with different amplitudes. The random *Track-Position* factor h(x) is then considered as the sum of individual harmonic unevenness with different wavelength λ_i and amplitude b_i:

$$h(x) = \sum_{i=1}^{k} b_i \cos\,(k_i x + \varepsilon_i), \tag{2.5}$$

where k_i is the wavenumber associated to each wavelength:

$$k_i = 2\pi/\lambda_i = \omega/v. \tag{2.6}$$

The wavenumber

$$k_i = 2\pi/\lambda_i \tag{2.7}$$

and the angular frequency

$$\omega = 2\pi v/\lambda \tag{2.8}$$

differ in the car velocity factor v:

$$\omega = k \cdot v \tag{2.9}$$

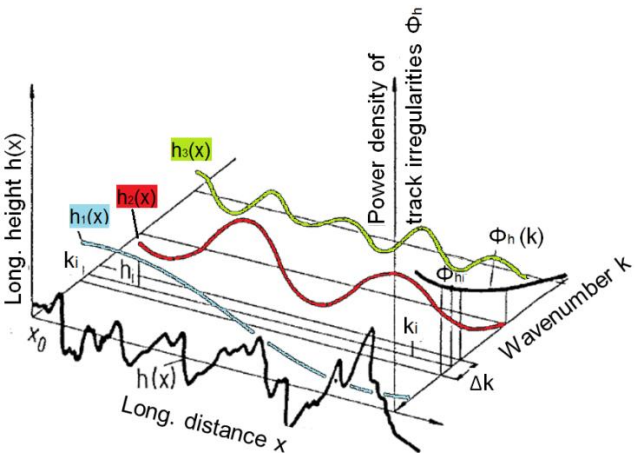

Figure 2.12: Track Position factor h(x) and the partial-irregularities of different angular wavenumber k associated *[6]*

Figure 2.12 shows the decomposition of the longitudinal height h(x) in the different harmonics $h_i(x)$ of different wavenumber that compose it. For an angular wavenumber k and a small wavenumber spectrum Δk, belongs a non-constant amplitude b_i. This amplitude changes along the distance x and depends on the wavenumber spectrum Δk size, and must, therefore, be written correctly as b_i (x, Δk). [6]

A descriptive parameter for the changing individual harmonic unevenness $h_i(x)$ is its variance σ^2_h:

$$\sigma^2_{h_i} = \frac{1}{n} \sum_{j=1}^{n} (h_j - \bar{h})^2 \tag{2.10}$$

The so-called *Power-Unevenness-Density* Φ_{hi} of the individual harmonic unevenness $h_i(x)$ and the wavenumber k_i is then defined as:

$$\Phi_{hi} = \frac{\sigma^2_{hi}}{\Delta k}, \text{ which dimension is } \left[\frac{cm^2}{rad/cm}\right]. \tag{2.11}$$

The variance σ^2_h is equal to the quadratic of the effective value of a specific individual harmonic unevenness $h_i(x)$

$$\sigma^2_{h_i} = (b_{eff_i})^2 \tag{2.12}$$

when the *Track-Position* factor h(x) is "accidentally constant" (the function has any exceptional individual value and any arbitrary interval of $h_i(x)$ owns equal mean values). Then, the *Power-Unevenness-Density* Φ_{hi} is written as:

$$\Phi_{hi} = \frac{(b_{eff_i})^2}{\Delta k} \tag{2.13}$$

The effective value b_{eff} and the amplitude b_i of the harmonic roughness-section $h_i(x)$ differ in a factor$\sqrt{2}$. Then:

$$b_i = b_{eff} \cdot \sqrt{2} \tag{2.14}$$

The application of a *Power-Unevenness-Density* average Φ_h on a wavenumber k induces *Power-Spectral-Density* $\Phi_h(k)$. This factor reveals which wavenumber k and which (mean square) amplitude b^2_{eff} are existing in a track. It is determined with *Track-Position* measurement signals, recorded with the adequate measurement method, obtaining then one graph per each *Track-Position* factor (h(x), u(x), s(x) and Ψ(x)). [6]

The Power-Density Φ(k) is taken with accumulative wavenumber k. That means that Track-Position-Errors appear with big wavelength and big amplitude, and the inverse, with small wavelength and small amplitude. The literature proposes remove *Power-Spectral-Density* Φ_h (k) within a wide distribution range, whose differ over and under the boundary of around decimal-power. The distribution range over the boundary is then defined as worst rail, on which a vehicle could ever meet. Analogous equivalent, under the boundary, the best rail is defined. The average rail position let between both extremes. The *Power-Spectral-Density* Φ_h (k) is a function of the wavenumber well approximated as a cubic hyperbola, and then written in the form:

$$\Phi[\mathrm{k}] = \frac{\mathrm{a}}{(\mathrm{b}+\mathrm{k}/2\pi[1/\mathrm{m}])^3} \tag{2.15}$$

With that, the description of so complex fact, as *Track-Position* with different amplitude and wavelength, is reduced of only two coefficients: a and b. The coefficient a is a measure of the Tail Position unevenness, while the coefficient b is a measure of the Track Position waviness. Big values of b mean a big percentage of shortly waves in spectrum. Table 1 contains the determined coefficients for rails, for worst, average and best rail position. [6]

Table 1: Different values of the rail coefficients to determine the Power-Density-Spectrum $\Phi_h(k)$ depending on the type of rail position: worst, average and best [6]

Track position		Worst		Average		Best	
longitudinal height	h	$9.39 \cdot 10^{-1}$	$6.89 \cdot 10^{-2}$	$1.31 \cdot 10^{-2}$	$2.94 \cdot 10^{-2}$	$1.90 \cdot 10^{-4}$	$9.71 \cdot 10^{-3}$
directional position	u	$2.74 \cdot 10^{-1}$	$3.13 \cdot 10^{-2}$	$1.33 \cdot 10^{-2}$	$2.33 \cdot 10^{-2}$	$6.33 \cdot 10^{-4}$	$1.3 \cdot 10^{-2}$
gauge	s	$1.64 \cdot 10^{-1}$	$5.35 \cdot 10^{-2}$	$4.68 \cdot 10^{-2}$	$7.96 \cdot 10^{-2}$	$1.23 \cdot 10^{-2}$	$1.12 \cdot 10^{-1}$
transverse position	Ψ	$2.16 \cdot 10^{-8}$	$1.19 \cdot 10^{-2}$	$2.87 \cdot 10^{-9}$	$3.17 \cdot 10^{-3}$	$4.07 \cdot 10^{-10}$	$5.57 \cdot 10^{-3}$

2.3.2 Spectral Synthesis

In the Spectral Analysis, *Power-Spectral-Density* Φ_h (k) is obtained from *Track-Position*, but *Track-Position* can also be reproduced from *Power-Density-Spectrum* Φ_h (k), as shown in Figure 2.13. This transformation is studied in the Spectral Synthesis. [6]

As said before, the longitudinal height h(x) is considered a synthesis of a lot of different harmonics $h_i(x)$ of different wavenumber with the amplitude bi and the phase angle εi:

$$h(x) = \sum_{i=1}^{k} b_i \cos\ (k_i x + \ \varepsilon_i) \tag{2.16}$$

The wavenumber k_i belonging to the amplitudes b_i are formed according to the *Power-Density-Spectrum* Φ_h (k):

$$b_i = \sqrt{\Phi_h(\mathrm{k}_i) \cdot \Delta\mathrm{k}} \cdot \sqrt{2}, \text{ with } \begin{cases} k_1 = k_0 \\ k_i = k_0 + (\mathrm{i}-1)\Delta\mathrm{k} \\ k_n = k_0 + (\mathrm{n}-1)\Delta\mathrm{k} \end{cases} \tag{2.17}$$

By the evaluation of the *Power-Spectral-Density* Φ_h (k), phase information lost will be recovered with the help of uniformly distributed random numbers R_i from 0 to 1. By the random numbers $0 \le R_i \le +1$, phase angle $0 \le \varepsilon_i \le 2\pi$ are asigned: $\varepsilon_i = 2\pi R_i$ [6]

Collecting all this information, the *Track-Position* factor h(x) can be obtaining applying the formula below:

$$h(x) = \sum_{i=1}^{k} b_i \cos[(k_0 + (\mathrm{i}-1)\Delta\mathrm{k})x + 2\pi R_i] \tag{2.18}$$

The obtained synthetic Track-Position is not identical to the original Track-Position. Both have however the absolute rail feature, what means that all the parameters are, for both Track-Position functions, absolutely equals. [6]

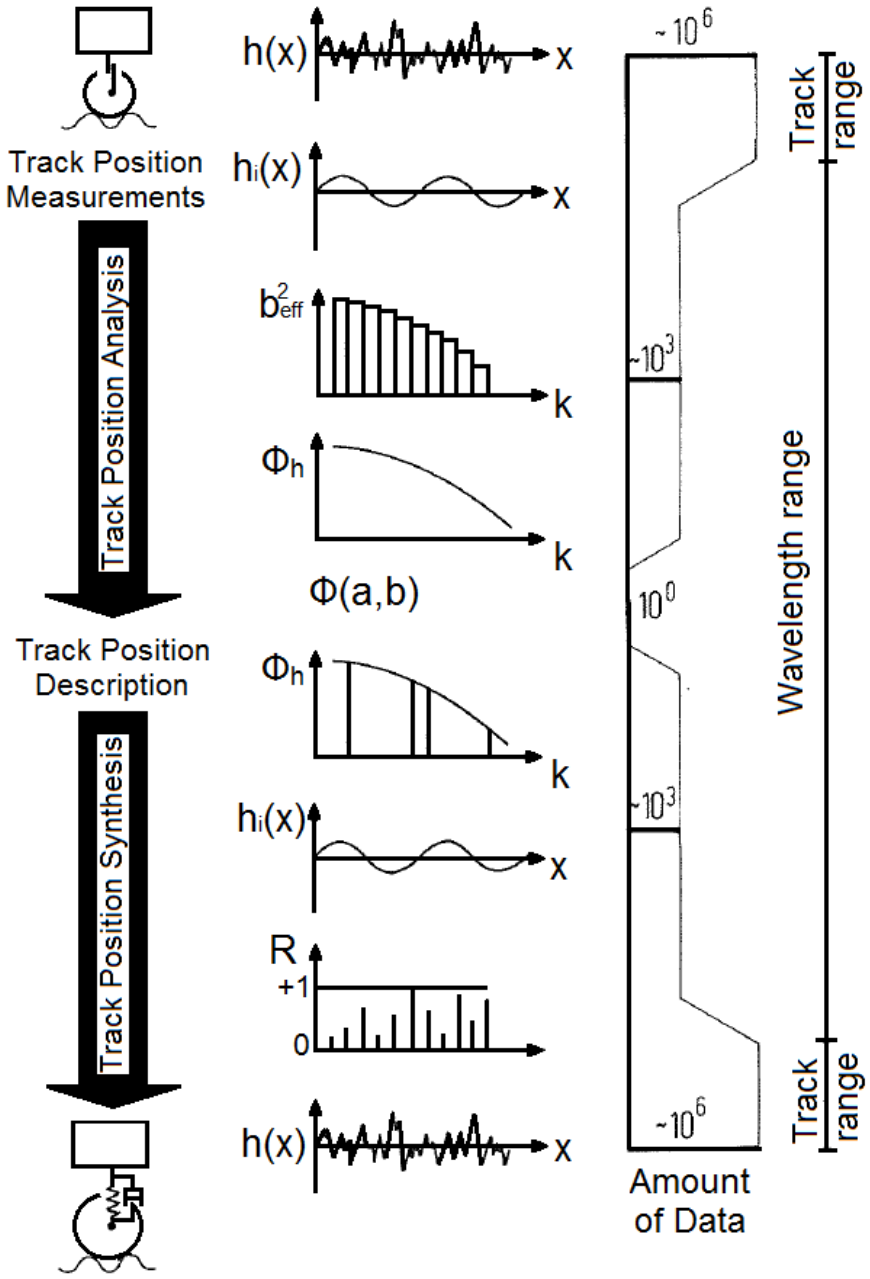

Figure 2.13: Steps to obtain the Power-Spectral-Density $\Phi_h(k)$ from the Track-Position (Spectral Analysis) and reproduction of the Track-Position from the Power-Density-Spectrum $\Phi_h(k)$ (Spectral Synthesis) [6]

2.4 Tramways composition

Trams are compact railway vehicle that runs on a track along public urban streets. They are designed to negotiate small radius curves and to improve accessibility of passengers. Because of that, trams are usually lighter and shorter than conventional trains. To achieve the possibility of running under small radius curves, an articulated arrangement is always needed. It can be achieved in several ways. There are two main articulated configurations (Figure 2.14). In the first case, the two bogies are directly coupled via an articulated bogie in between. The construction of this bogie is such that the two wheelsets rotate independently when passing a curve. In the second case, the coupling is achieved by a shorter bogie section in between the two main cars, mounted over a normal non-articulated bogie, in such a way that body section and bogie rotate together when passing a curve. [1, p. 72]

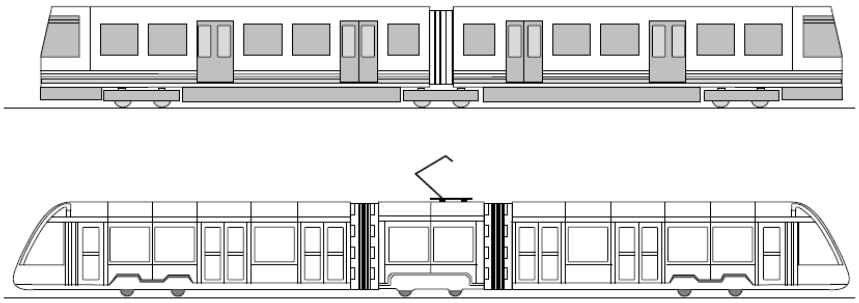

Figure 2.14: Different articulated tram configurations [1, p. 72]

The distance between the tram floor and the rail is different depending on the tram. In low-floor trams, it is about 300-350 mm, while for the high-floor it is usually 560 – 600 mm. Regarding this factor, there are two main types of tram: *Partially low-floor trams* have the ratio of low floor at least 50% of the total length of the floor, while *Fully low-floor trams* have low-floor bogies to achieve a whole floor at a height of 300-350 mm above the top of the rail. A new configuration is the so called *Ultra low-floor tram (ULF),* with the smallest distance between floor and rail, about 18 cm. [11][12][13]

2.4.1 Yaw Movement

The configuration of the wheels attachment can be rigidly attached (wheelset) or with independent wheels, see Figure 2.15. In a wheelset configuration the wheels have the same angular speed and a constant distance between them. When a wheelset enter in a curve, the inner wheel has a smaller curve radio, resulting in a higher velocity of this wheel. Since the wheels are joint rigidly by the axle, this different velocity is translate into

a different effective wheel radio, Figure 2.16. Because of that, a wheelset performs a sinusoidal movement called hunting oscillation. Figure 2.15.a. [1, p. 40-41]

The origin of this movement is the combination of two facts, the conic wheel shape and the creep forces acting between the wheels and the rails when running straight at high speeds. These facts turn into a combined action of longitudinal and lateral wheel-rail contact forces, that finally results in a coupled lateral and yaw vibration of the bogie.

The main problem of this movement appears at a speed known as “critical speed”. Below this speed, the motion is damped out, but above it, this motion becomes unstable. Under unstable conditions, very large amplitudes of vibration take place. These vibrations cause flange contact of the wheels on the rails, potentially causing derailment, and big forces on the rail, with the risk of induce permanent deformations. [7][8]

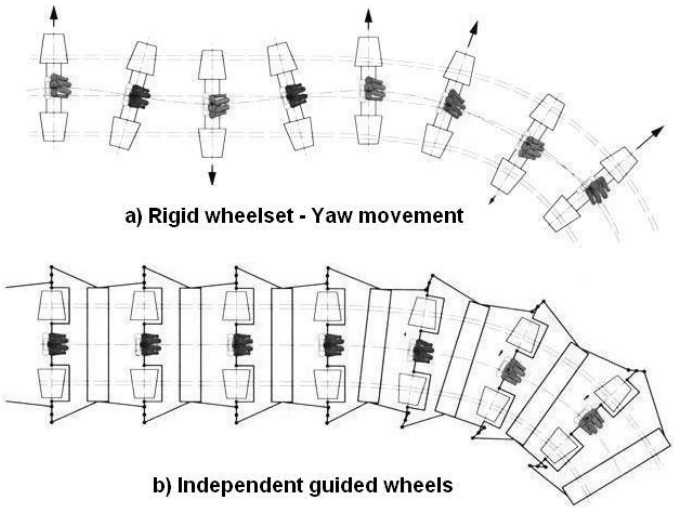

Figure 2.15: Difference between rigidly wheelset (a) and independents wheels (b) [30]

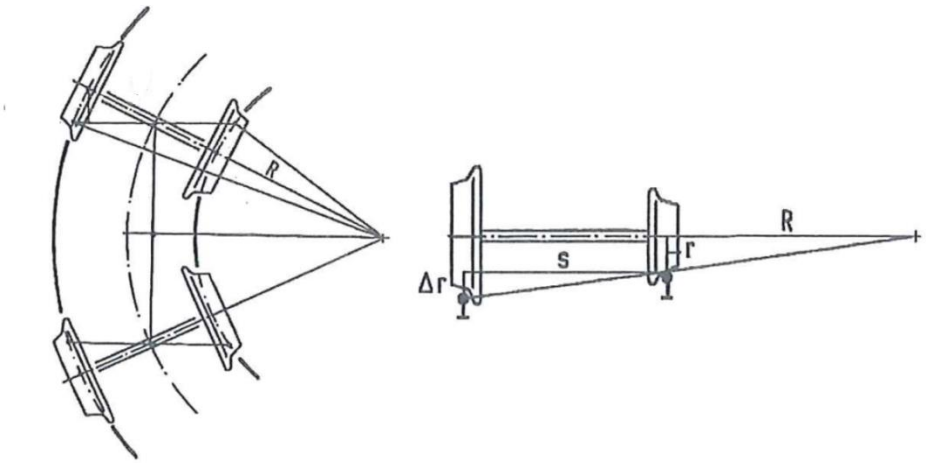

Figure 2.16: Effect of conical wheel shape when taking a curve. [34]

In a bogie with independent wheels, yaw movement is avoided and therefore, the train instability is minimized. In that case, an external mechanism is required in order to guide the wheels and keep the angle between the wheels and the rail at around zero, see Figure 2.15.b. [7][8]

2.4.2 Multi-Articulated-Vehicles

The conflict between the needed of a high length of the railway and the large curvature of many railway lines is usually solved by providing multi-articulated configuration (several trailer body sections carried by a first motor carbody). Compared to older tramways, the permanently attachment between body section and articulation turns into some advantages and disadvantages. They are based on less number of body-sections and length of them. Usually such wagons behave good while running straight or through a well-built translation curve and provide an excellent use of space, because they do not require extra space to rotate. This is a big advantage mainly when running through narrow track and closed curves. They also use an optimal envelope curve, which causes small gap in between railway and platform when stopping in curves. But this configuration also turns into higher axle loads and higher costs, due to the fact that each additional carbody means money (traction, brake). A general configuration of a Multi-articulared vehicle is shown in Figure 2.17. [32, p. 48] [33, p. 320-324]

The most common problem in the use of multi-articulated vehicles comes when talking about the angle described by each body-section. There is a deviation of the angle described by each carbody compared to the previous while running through a curve. This turns into a big difference when talking about the angle of the last body section compared to the motor carbody. This, plus the fact that on multi-articulated vehicles the sinusoidal movement well known as hunting oscillation is also transmitted along the length of the vehicle, makes very important the study of the lateral movement of the last carbody. This movement can be minimized by introducing damping between carbodies. A common solution is the introduction of two parallel longitudinal inter-car dampers. [1, p. 11; p. 390] [33, p. 320-324]

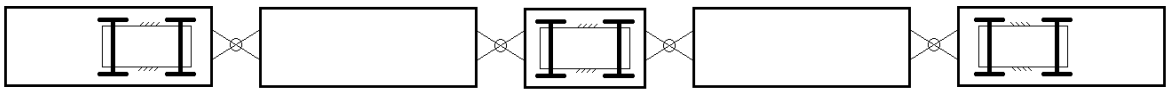

Figure 2.17: Multi-articulated vehicle configuration. D.t. [34]

2.4.3 Yaw Dampers

As have been mentioned before, there is a critical speed that appears due to kinematic oscillation (yaw motion) of a railway vehicle. All vehicles should operate well below their critical speed**.** Therefore, the critical speed is one of the main limiting factors to the increase of railway speed, and, therefore, the main goal is to increase this speed.

The usual way followed to increase the critical speed of railway vehicles is the use of yaw dampers. They are placed in two positions: between carbodies and bogies and between two cars in articulated vehicles (intercar damper, see Figure 2.18). The goal of the first one is to minimize the transmission of the yaw movement between these two structures; and their characteristics are chosen to achieve a balance between dynamic stability and low wheel–rail forces during curve negotiation. Intercar dampers are placed to minimize the transmission of the movement along the length of the vehicle. The vertical position of these intercar yaw dampers can be at floor or roof level. Figure 2.19 shows an example of railway vehicle with both types of damper. [15, p. 231]

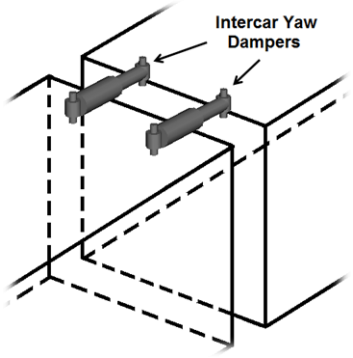

Figure 2.18: Intercar yaw damper placement

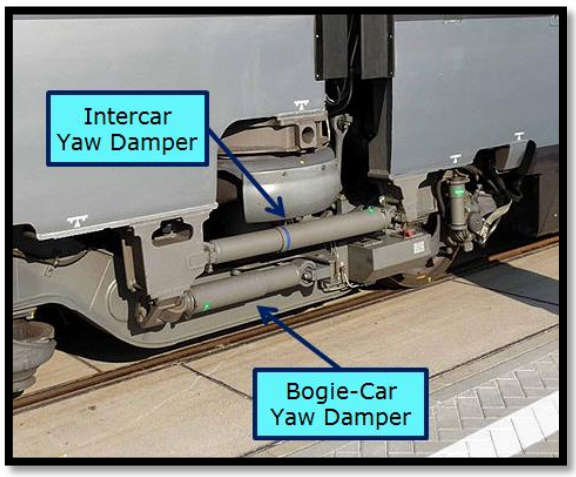

Figure 2.19: Example of Intercar and Bogie-Car Yaw Dampers [31]

2.5 Composition of the Combino

The Combino Trams are multi-articulated vehicles that can be found in different configurations. The two principal models are three-section and five-section, both with 100% low-floor tramcars, as shown in Figure 2.20. The configuration under study in this work is the second one, and it is in which this section is going to be focused. [28]

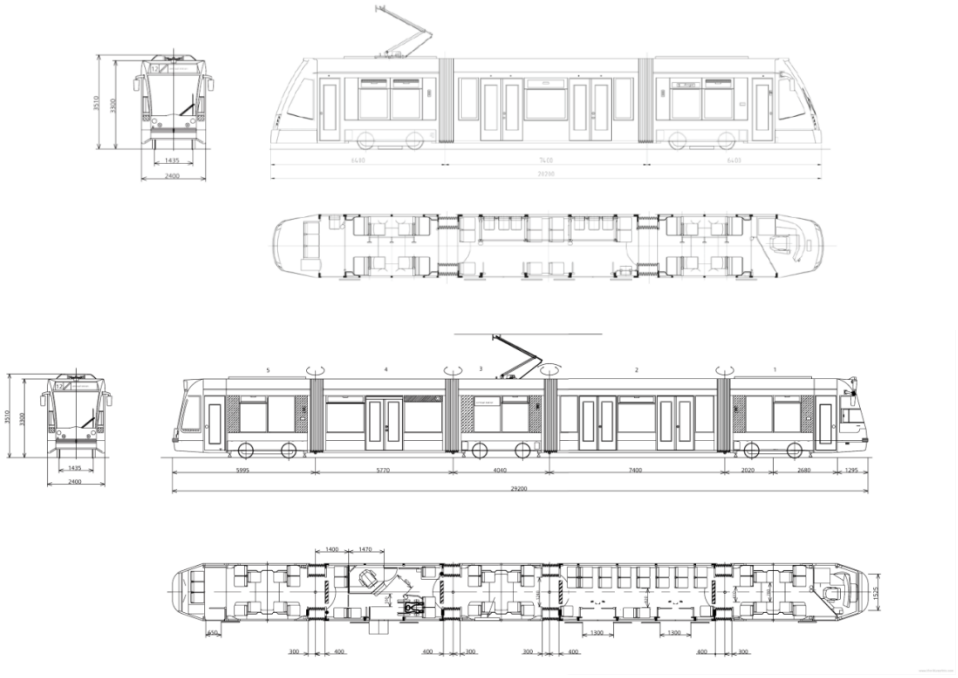

Figure 2.20: Three-sections and four-section Combino tramways configurations [28]

On the five-section Combino three bogies are mounted. The one in the middle is a trailer bogie (non-motorized bogie), while the two on the sides are motor bogies, both design for low-floor tram cars, as shown in Figure 2.21.

Figure 2.21: Two different configurations for Combino bogies, Trailer (left) and Motor (right) [29]

The configuration of the bogies (well-done explained in section 2.1.3.) is: independent wheels for the trailer bogie; and longitudinal wheelset, with the coupling done by two motors, one on each side, and four gearbox coupling, for the motor bogies. One the first case, each wheel has an independent angular velocity, while for the motor bogie the two wheels of the same side have the same angular velocity.[29]

Some important parameters of the five-section Combino are shown in

Table *2*.

Table 2: Five-section Combino technical data [28]

Vehicle Unit	**Five-section, low floor articulated COMBIMNO tram**
Track gauge	1435 mm
Vehicle length	3535 mm
Vehicle width	2650 mm
Weight empty	35,3 t
Max. speed	70 km/h
Low-floor component	100%
Floor height	300 mm

2.6 Load assumptions

2.6.1 Theory of signals, loads and fatigue

If a function represents a physical quantity or variable containing the information about the behavior and nature of the phenomenon, it is known as a signal. [21, p. 7]

The main characteristics of a signal are its amplitude and period. From these two, range, mean and frequency are defined, see Figure 2.22. A pair consisting of a minimum and maximum defines a cycle, where the range is the most important characteristic for fatigue evaluation. Full cycle means that the load goes from a minimum to a maximum and then back again to the minimum. It consists of two half-cycles, a term useful in fatigue analysis. [22, p. 40]

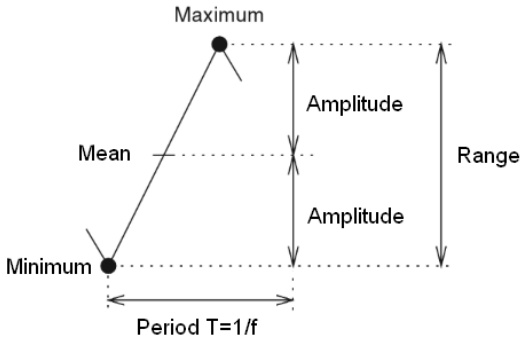

Figure 2.22: Main values that define a signal [22, p. 40]

There are two main classifications of signals, continuous time signal and discrete time signal, see Figure 2.23. If a signal is defined at all values of t, where t is a continuous variable, this is known as a continuous time signal; while the discrete time signals are obtained at sampling instants. [21, pp. 7-21]

A load is a physical quantity that reflects the excitation of a system over the time. The most typical loads are forces, torques, stresses, strains, displacements, velocities and accelerations. It is usually a measured discrete time signal, where only a certain discrete points in time are known, called load history. [22, pp. 33-34]

The simplest kind of load condition is the constant amplitude load, Figure 2.24.a. Consider block loads with same amplitude each block is the next generalization, as shown in Figure 2.24.b. In reality, the loads that are measured are variable amplitude loads, see Figure 2.24.c and Figure 2.24.d. [22, pp. 15-17].

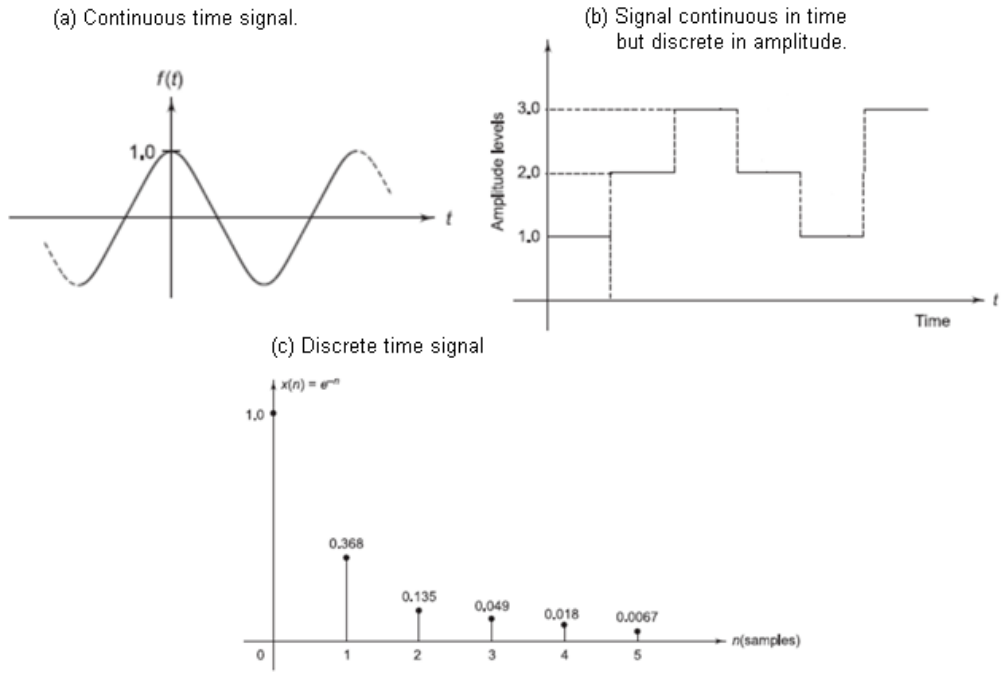

Figure 2.23: Classification of signals. Continuous (a) and discrete (c) time signals [21, p. 7]

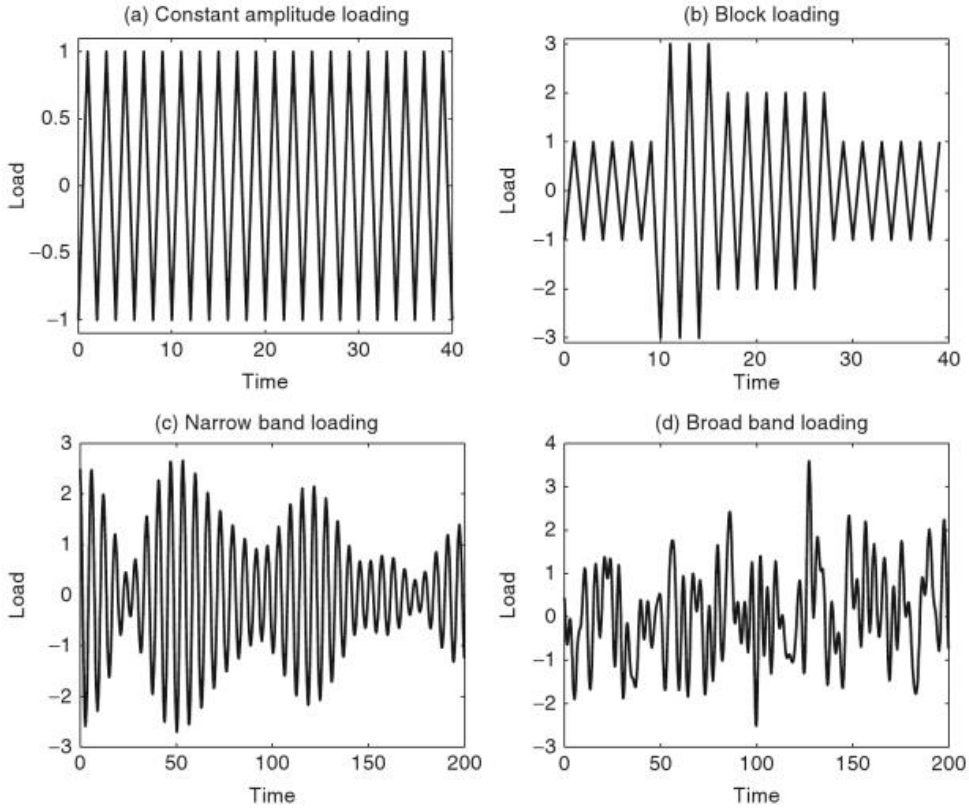

Figure 2.24: Different type of loads. (a) Constant amplitude loading. (b) Block loading. (c) Narrow band loading. (d) Broad band loading. [22, p. 15].

"Fatigue is the progressive and localized structural damage that occurs when a material is subjected to cyclic loading" [23, pp. 57-58]. When the stresses are not above the elastic limit, a given load condition may be repeated even a few hundred times without the appearance of structural problems. However, when loadings are repeated thousands or millions of times, rupture will occur at a stress much lower than static breaking strength. This phenomenon is known as fatigue [24, p. 6] and it is the result of the cumulative process consisting of crack nucleation, short crack growth, long crack growth, and final fracture of a component. [23, pp. 57-58]

A fatigue load is generally represented by a cyclical waveform called S-N curve. The quantity S usually represents stress, while N represents the number of cycles to failure. [25, pp. 4-5].

The aim of the methods is to understand and describe the load properties that are important for fatigue in durability analysis. We distinguish two types of methods: Amplitude-based methods or rate independent methods only depend on the sequence of the local extreme values in the signal without taking into account the time between maximum and minimum peaks. Frequency-based methods or rate-dependent methods take into account the "speed" of the signal and are very useful for system load analysis. [22, pp. 33-34].

The transformation from external load (where the load is applied) to local loads (where you are going to analyze) should be also take into account to decide the method to use. The further you are analyzing from the original point of loading, the more you have to go to frequency analysis [22, p. 23]. The direction of analysis of each method is shown in Figure 2.25.

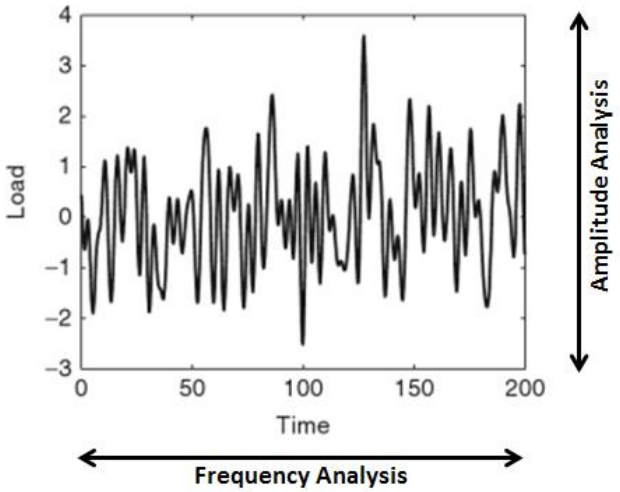

Figure 2.25: Amplitude and Frequency analysis methods. Direction of analysis.

2.6.2 Amplitude-based methods

To know the fatigue life of a structure, first is needed to know the corresponding cycle loading absorbed by the structure. In reality, structures are usually subjected to complex loading (non-constant amplitude load), being difficult to determine what constitutes a cycle and the corresponding amplitude of that cycle.

Cycle counting *algorithms* are used to reduce a complicated variable amplitude loading history into a number of discrete simple cycles, which are associated with fatigue damage, by pairing the local maxima with the local minima. These algorithms are followed explained. [22, p. 17; pp. 33-34] [23, p. 78]

After apply these methods we obtain a block loading condition. To analyze the number of cycles before the fracture of the component, Palmgren-Miner rule is used. This method assumes that each cycle with amplitude S uses a fraction 1/N of the total life. [22, p. 16] [24, p. 24]

The process follow to evaluate the fatigue life of a structure is shown in the diagram below (Figure 2.26).

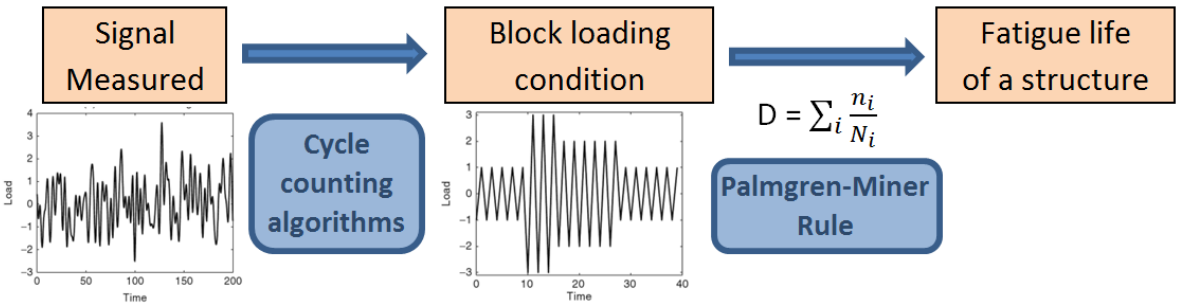

Figure 2.26: Amplitude methods. Flow Chart of execution.

The main cycle counting methods used are: Level-crossing, Peak-valley, Range-mean Range-par and Rainflow. The Rainflow counting method is generally accepted as being the best cycle counting algorithm. Examples of each method are explained in Annex A. All of them are below explained. [22, p. 17]

For a better understanding of each method, an example of them is explained on each case. Figure 2.27shows the load history that is going to be analyze on these examples. The data of this load has been taked from [22, p. 36].

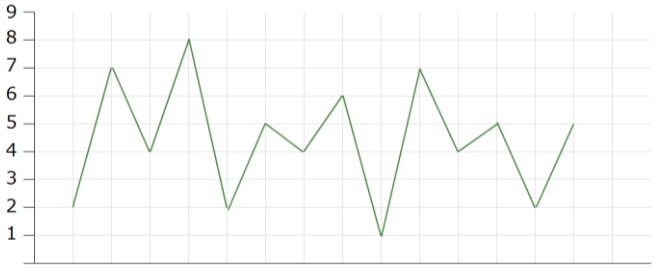

Figure 2.27: *Load History to analyze*

In some cases, only peaks that are above or below a certain load level may be of interest for a life prediction. Usually, this reference level is determined by the mean of the complete load-time history. In those cases, *Level Crossing Cycle Counting* methods is employed. One count is defined when a portion of the load-time history with a positive slope passes above the reference load level or when a portion with a negative slope crosses below it. The final cycle is determined by joining all the counts counted, from the largest to the smallest. An example of this method is shown in Figure 2.28 [23, pp. 78-79] [25, p. 79]

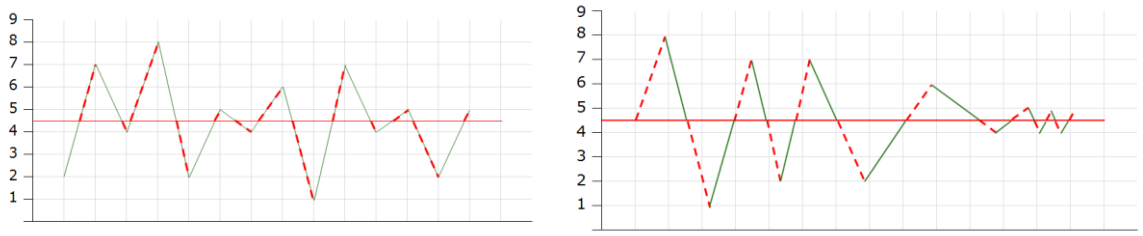

Figure 2.28: Level Crossing Cycle Counting

Peak-Valley Cycle Counting identifies the maxima and minima in a load-time history, where a maxima is the transition point between positive and negative slop, and minima is the opposite. Maxima above and minima below a reference load level are counted. As in the previous method, the final cycle is determined by joining all the counts counted, from the largest to the smallest. An example of this method is shown in Figure 2.29 [22, p. 56] [23, pp. 79-80].

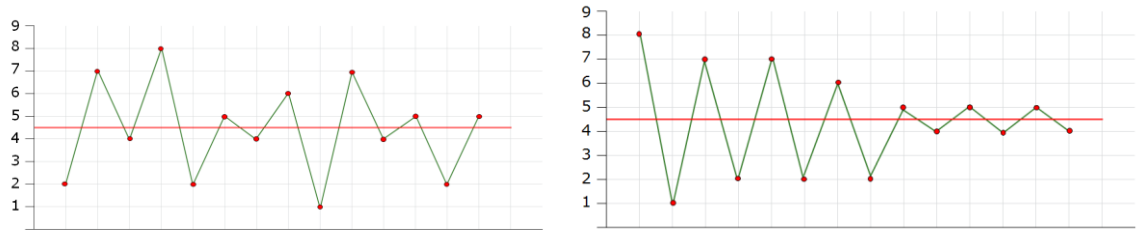

Figure 2.29: Peak-Valley Cycle Counting

Markov Counting and *Range-Mean Counting,* are close related. The first one, pairs consecutive locals maxima and minima along a load spectrum, obtaining cycles, while the second extract the ranges of these cycles and counts the times each range appears. Each range represents one-half cycle. Positive ranges are defined on positively sloped and negative ranges on negatively sloped ranges. An example of this method is shown in Figure 2.30 [22, pp. 51-54]

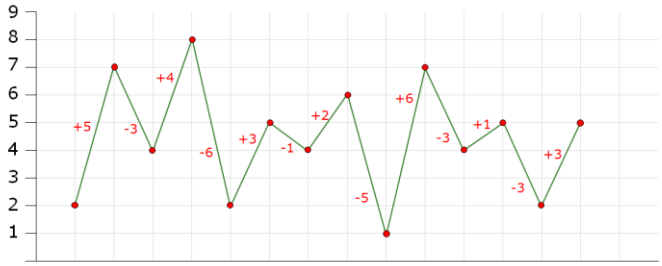

Figure 2.30: Markov & Range-Mean Counting

The only two methods with a direct relation to hysteresis cycles are *Rainflow Cycle Counting* and *Range-Pair Cycle Counting.* While the first counts the cycles along a load history, the second extracts the ranges of these cycles.

Rainflow Cycle Counting (RFC) is the generally accepted and recommended procedure for estimation of fatigue damage of structures submitted to random loading. RFC method was first introduced in 1967 to count the cycles or the half cycles of strain-time signals and has since then become the most commonly used cycle counting method in engineering.

The RFC method was designed to catch both slow and rapid variations of the load by forming cycles that pairs high maxima with low minima even if they are separated by intermediate extremes. [24, pp. 13-14] [25, pp. 80-83] [26, pp. 160-161].

The original definition of the RFM is the *Pagoda Roof Method. On it, w*ith the time axis in vertical, the random stress S(t) represents a series of roofs on which water falls. The drop will stop either if it meets an opposing peak larger than that of the start or if it meets the path traversed by another drop, previously determined. The drop can fall on another roof and continue according to previous rules. The same rules are followed to define rainflows in valleys. The horizontal length of each rainflow defines a range equivalent to a half-cycle of a constant amplitude load. [24, pp. 15-22]

The RFC method starts from a process of peaks and valleys. Then the time axis is rotated so that it points downward. At both peaks and valleys, water sources are considered. Water flows downward according to the following rules:

1. A rainflow path starting at a peak/valley will continue down the “pagoda roofs”, until it encounters a peak/valley that is more positive/negative than the origin. From the Figure 2.31, the path that starts at A will end at E.
2. A rainflow path is terminated when it encounters the flow from a previous path, Figure 2.31, see paths C, I and K.
3. Peak/Valley-generated half-cycles are defined for the entire record. For each cycle, the stress range S_i is the vertical excursion of a path. The mean S_i is the midpoint.
4. For a sufficiently long record, each valley-generated half-cycle will match a peak-generated half-cycle to form a whole cycle. [24, pp. 15-22]

The example of application of the *Pagoda Roof Method is shown in* Figure 2.32.

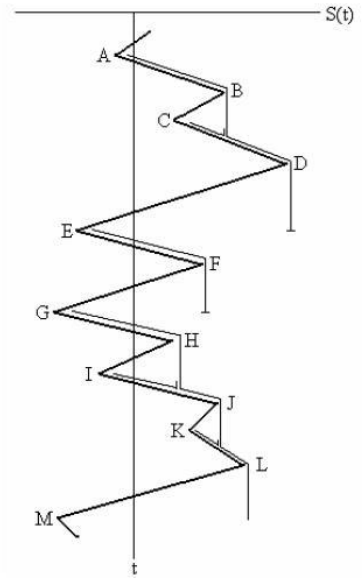

Figure 2.31: RFC method. Rainflow paths [24, p.19]

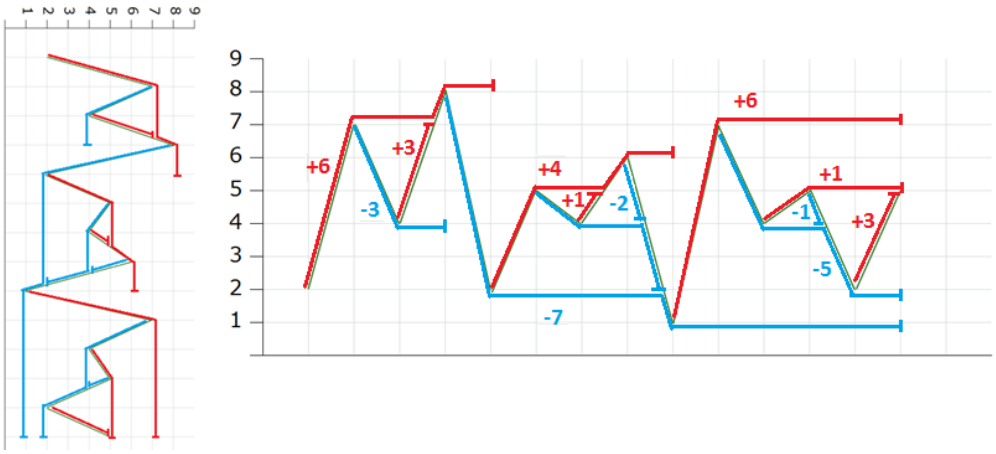

Figure 2.32: RFC – Pagoda Roof Method

The practical definition of the RFC is the *4-Point Algorithm. On it, s*tarting with the first 4 points of a sequence of discretized points where the minima-maxima filtering has been done, cycles are counted following the formula of Figure 2.33.

If $[(\min(s_1, s_4) \leq \min(s_2, s_3)) \;\&\&\; (\max(s_2, s_3) \leq \max(s_1 = s_4))]$
then the pair (s_2, s_3) is a cycle.

Figure 2.33: 4-Point Algorithm [22, p. 43]

In case the pair is not taken as cycle, the next four min-max are chosen as current points, moving one position following the time sequence. In case the pair is taken, it is stored in the rainflow matrix RFM, the points are removed from the stack and the four new points are initialized, taking again the first four. Then the counting rule is applied again until the last point of the time signal is reached. After that we obtain a rainflow matrix (RFM) with the cycles counted, and a residual RES with the remaining sequence of points.

If a local stress history is applied once, some hysteresis cycles will result from that, while applying it a second time, some other cycles will be created. The firs hysteresis cycle exist only once, while if the signal is applied further, the same cycles as during the second run will be created. That is called first and second round cycles, both stored in the RFM. The second round is of high importance and can be obtained by doubling the residual and making the 4-point algorithm to it. An example of this method is shown from Figure 2.34 to Figure 2.46. [22, p. 43-47]

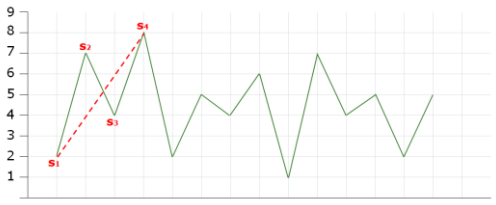

Figure 2.34: RFC - 4-point Algorithm. 1st iteration: $s_1 = 2$, $s_2 = 7$, $s_3 = 4$, $s_4 = 8$; RFM = [(7,4)] => Pair counted.

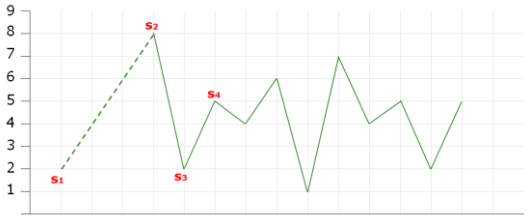

Figure 2.35: RFC - 4-point Algorithm. 2nd iteration: $s_1 = 2$, $s_2 = 8$, $s_3 = 2$, $s_4 = 5$; RFM = [(7,4)] => Pair not counted.

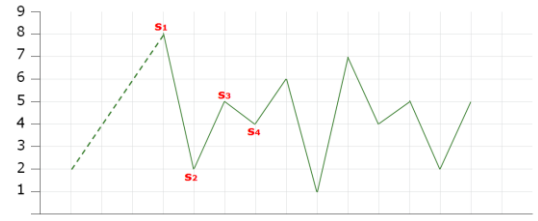

Figure 2.36: RFC - 4-point Algorithm. 3rd iteration: s1 = 8, s2 = 2, s3 = 5, s4 = 4; RFM = [(7,4)] => Pair not counted.

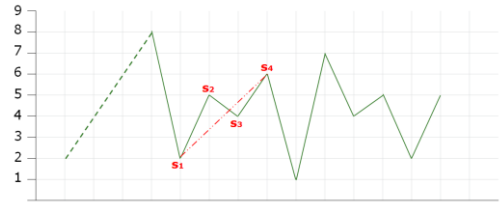

Figure 2.37: RFC - 4-point Algorithm. 4th iteration: $s_1 = 2$, $s_2 = 5$, $s_3 = 4$, $s_4 = 6$; RFM = [(7,4),(5,4)] => Pair counted.

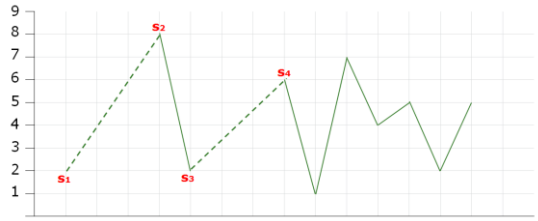

Figure 2.38: RFC - 4-point Algorithm. 5th iteration: s1 = 2, s2 = 8, s3 = 2, s4 = 6; RFM = [(7,4),(5,4)] => Pair not counted.

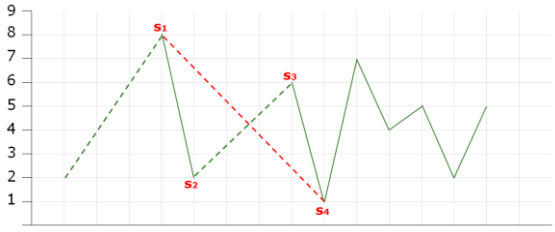

Figure 2.39: RFC - 4-point Algorithm. 6th iteration: $s_1 = 8$, $s_2 = 2$, $s_3 = 6$, $s_4 = 1$; RFM = [(7,4),(5,4),(2,6)] => Pair counted

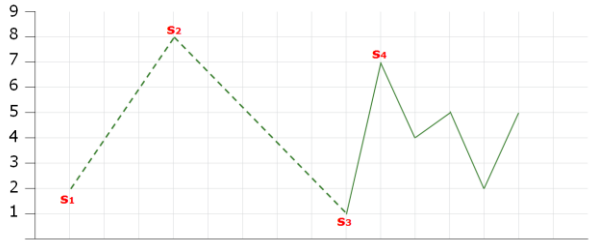

Figure 2.40: RFC - 4-point Algorithm. 7th iteration: $s_1 = 2$, $s_2 = 8$, $s_3 = 1$, $s_4 = 7$; RFM = [(7,4),(5,4),(2,6)] => Pair not counted.

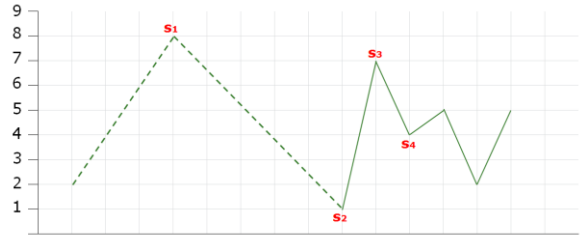

Figure 2.41: RFC - 4-point Algorithm. 8th iteration: s_1 = 8, s_2 = 1, s_3 = 7, s_4 = 4; RFM = [(7,4),(5,4),(2,6)] => Pair not counted.

Figure 2.42: *RFC - 4-point Algorithm.* 9th iteration: s_1 = 1, s_2 = 7, s_3 = 4, s_4 = 5; RFM = [(7,4),(5,4),(2,6)] => Pair not counted.

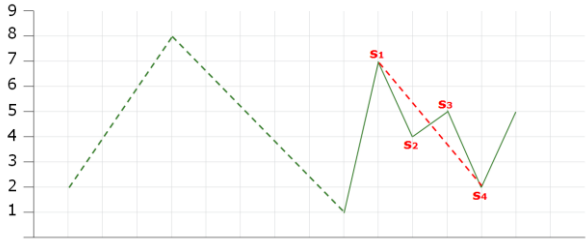

Figure 2.43: RFC - 4-point Algorithm. 10th iteration: s_1 = 7, s_2 = 4, s_3 = 5, s_4 = 2; RFM = [(7,4),(5,4),(2,6),(4,5)] => Pair counted.

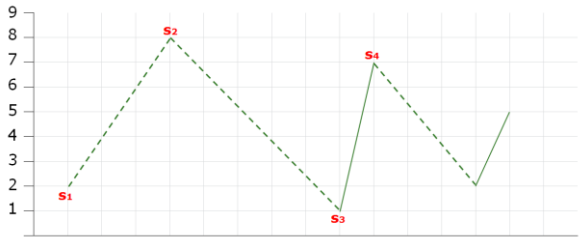

Figure 2.44: RFC - 4-point Algorithm. 11th iteration: s_1 = 2, s_2 = 8, s_3 = 1, s_4 = 7; RFM = [(7,4),(5,4),(2,6),(4,5)] => Pair not counted.

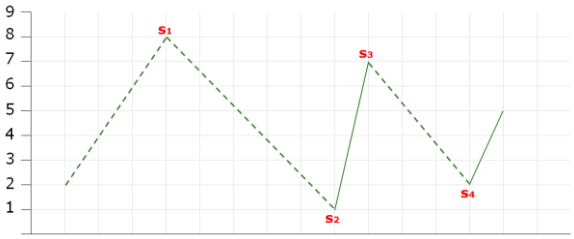

Figure 2.45: RFC - 4-point Algorithm. 12th iteration: s_1 = 8, s_2 = 1, s_3 = 7, s_4 = 2; RFM = [(7,4),(5,4),(2,6),(4,5)] => Pair not counted.

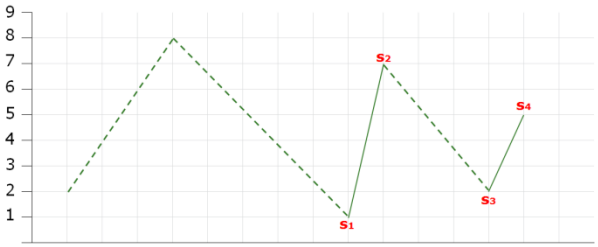

Figure 2.46: RFC - 4-point Algorithm. 13th iteration: s_1 = 1, s_2 = 7, s_3 = 2, s_4 = 5; RFM = [(7,4),(5,4),(2,6),(4,5)] => Pair not counted.

The *Range-Pair Cycle Counting* extracts the ranges of the cycles along a load history counted by RFC with 4-point algorithm. It stores in a vector the number of times each range is repeated. It is done following the formula below:

$$f^{rp}(k) = \sum_{|i-j|=k} RFM\ (i,j) + contribution\ from\ RES \qquad (2.19)$$

However, it is usually presented in cumulative form, where at level k all cycles with a range greater than k are shown. An example of application of this method is shown in Figure 2.47. [22, p. 49]

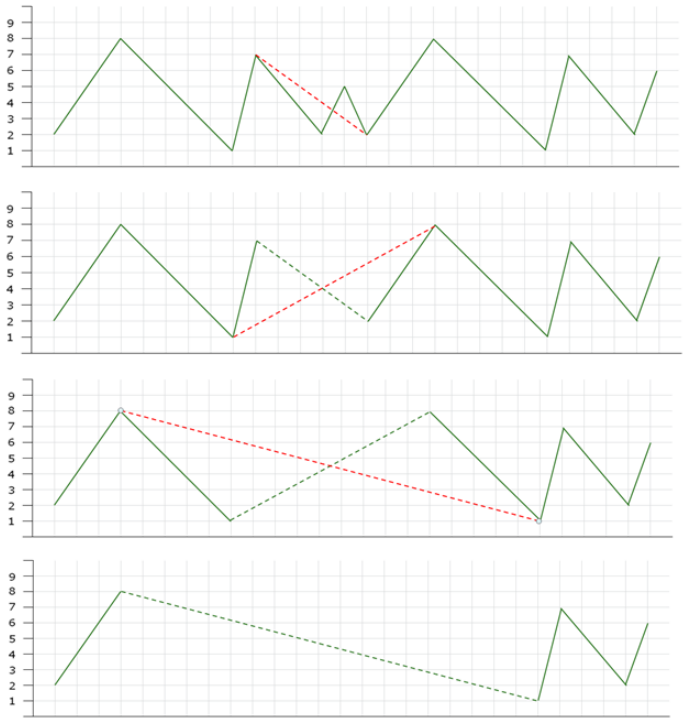

Figure 2.47: Range-Pair Cycle Counting

The result of the cycles counted by each method on the example of applicacion is shown in Table 3.Table 4 shows the Cycles counted applying each cycle counting method grouped by range, while Table 5 shows the same results in cummulative form.

Table 3: Cycles counted applying each Cycle Counting Method

Cycle Counting Method	**Cycles counted**	
	Full cycles counted	Half cycles counted
Level Crossing	(1,8), (7,2), (7,2), (5,4), (5,4)	(6,3), (5,4)
Peak Valley	(1,8), (7,2), (7,2), (5,4), (5,4)	(6,3), (2,7), (5,4)
Rainflow Matrix 4-P.A	RFM = [(7,4),(5,4),(2,6),(4,5)]; RES = (2,8,1,7,2,5)	
Range-Pair	RFM = [(7,4),(5,4),(2,6),(4,5)]; RES = [(2,5), (7,2), (1,8)]	

Table 4: Cycles counted applying each cycle counting method grouped by range.

		Results						
Method	Range	1	2	3	4	5	6	7
Level Crossing Cycle Counting	Cycles counted	2,5	0	0,5	0	2	0	1
Peak-Valley Cycle Counting		2,5	0	0,5	0	2,5	0	1
Range-Mean Counting		1	0,5	2,5	0,5	1	1	0
RFC – Pagoda Roof Method		1,5	0,5	1,5	0,5	0,5	1	0,5
RFC – 4-point Algorithm => Range-Pair Cycle Counting		2	0	2	1	1	0	1

Table 5: Cumulative cycles counted applying each cycle counting method grouped by range.

		Results							
Method	Range	0	1	2	3	4	5	6	7
Level Crossing Cycle Counting	Cycles counted	6	3,5	3,5	3	3	1	1	0
Peak-Valley Cycle Counting		6,5	4	4	3,5	3,5	1	1	0
Range-Mean Counting		6,5	5,5	5	2,5	2	1	0	0
RFC – Pagoda Roof Method		6	4,5	4	2,5	2	1,5	0,5	0
RFC – 4-point Algorithm => Range-Pair Cycle Counting		7	5	5	3	2	1	1	0

All the methods can be easily compared using Table 6. The main different in between methods is if they are related or not to the hysteresis cycles. In case they are, these results are a good approximation for durability evaluation. The two main methods to extract the cycles are RFC (hysteresis related) and Markov Counting (Not hysteresis related). From the result of those two, Range-Pair and Range-Mean are apply respectively. Level Crossing and Peak-Valley can be also hysteresis cycles related if the extraction of the information is done from the cycles counted using RFC. The relation between all the methods is shown in Figure 2.48.

Table 6: Comparison of different cycle counting methods.

NAME	METHOD	OUTPUT	APPLICATION	HYSTERESIS CYCLES RELATION
Rainflow Cycle Counting	Counts rainflow cycles using a specific algorithm. The 4-point algorithm is the most recommended.	Hysteresis cycles in the load	**Durability** evaluation	Yes
Markov Counting	Counts cycles by pairing consecutive local maxima and minima. (For narrow bands similar results than using RFC).	Cycles in the load.	The most straightforward method for counting cycles.	No
Range-pair Counting	Extracts the cycle ranges of the RFC.	Rainflow amplitudes distribution.	Used together for comparison of signals (they have complementary load information)	Yes
Range-Mean Counting	Extracts the cycle ranges of the Markov C.	Cycles amplitude distribution		No
Level Crossing Counting	Counts the number of times the load crosses a certain load level.	Mean values cycles distribution		-
Peak-Valley Cycle Counting	Identifies the maxima and minima in a load. (transition points between positive- negative slop)	Max/min above/below a reference load level.		-

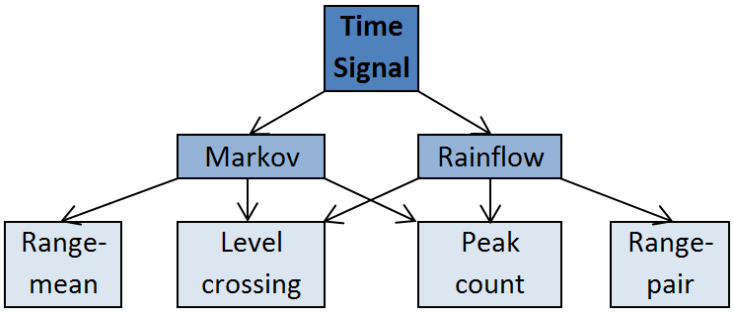

Figure 2.48: Relation between different counting methods [22, p. 72]

2.6.3 Frequency-based methods

As was briefly explained before in Section 2.6.1, frequency analysis has to be done when the analysis takes place far from the original point of loading; while amplitude domain is most important at local stress and strain level. On this study of the Combino, it is assumed that the distance between where the load takes place and where the durability study is needed is negligible. For that reason frequency-based methods are not going to be deeply explained.

When non-local quantities are processed, all the properties of the loads which have an influence on the local stress have to be take into account. If this is the case, to the amplitude domain of the outer loads, which still having a big importance, we have to add the importance of the frequency behavior or spectral properties. [22, p. 23; p. 72]

A Power Spectral Density (PSD) function is the most common way of representing the loadings or responses in the frequency domain. PSD represents the energy of the time signal at different frequencies. Direct methods achieve prediction of fatigue damage from an output PSD of stress response. These techniques are divided in two categories, those that estimate fatigue life directly and those that compute range mean histograms as an intermediate stage. [23, p. 369-371] [27, p. 1-4]

Generally, stress data is reported in time domain, but sometimes, this is not the case, and the load history is plotted in the frequency domain. An example of both kind of representations is shown in Figure 2.49. Depending of the kind of analysis needed, this can be an inconvenient. Following, it is described how to go from time domain representation to frequency domain and vice versa. [23, p. 369-371] [27, p. 1-4]

When we are in front of a PSD representation, and an amplitude analysis is needed, a characteristic time history has to be regenerate from it, to proceed afterwards with one of the amplitude-based methods describe above. To do that, a series of computational algorithms based on Fourier analysis techniques has been developed. The transformation between time domain and frequency domain is obtain using the Fast Fourier Transform (FFT), while the Inverse Fourier Transform (IFT) can be used to transform the frequency-based signal to the time-based loading. When starting with a PSD this method is not exact because the PSD does not contain any of the original phase information. For certain time histories, however, we are able to make assumptions about the original phase content and therefore regenerate a statistically equivalent time history. To regenerate a time signal from a PSD we therefore assume that the original process was stationary, Gaussian and random. Then, random phase angles can be generated and added to the

amplitude data given in the PSD. At this point we use the Inverse Fourier Transformation to determine a statistically equivalent time history. [23, p. 369-371] [27, p. 1-4]

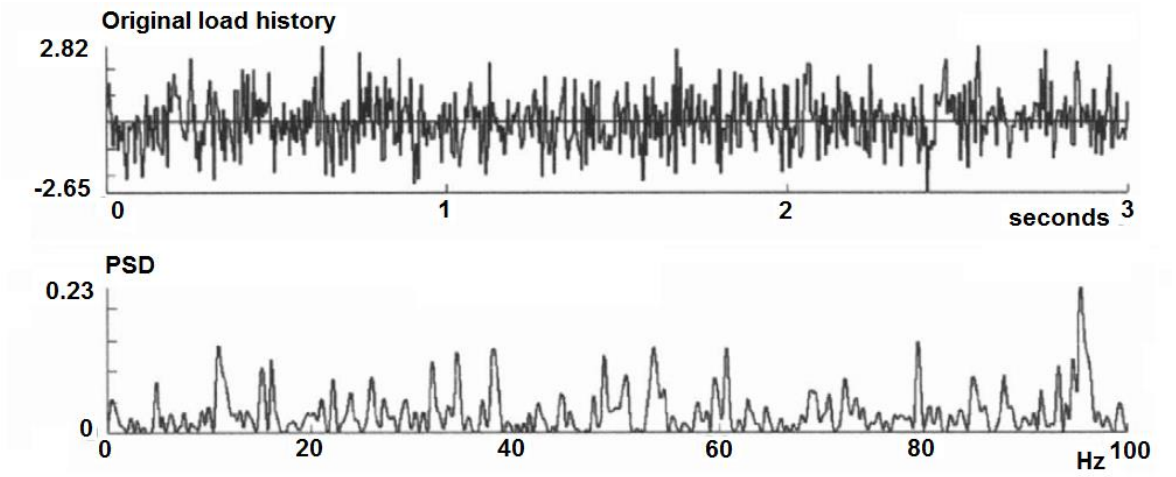

Figure 2.49: Time and Frequency domain signals [23, p. 379]

2.6.4 Rainflow Matrix

In section 2.6.2 is explained how to obtained the cycles of a load history and to store them in a matrix. From this point, a better representation of this information is useful for future analysis. This matrix is well known as Rainflow Matrix (RFM). A deeper explanation of this matrix is needed to understand its functionality and utility.

Once the cycles are counted using one of the methods explained below, the first representation of the RFM is done. First, the signal is discretized to 32 levels, equally spaced and then the cycles counted are classified into the rainflow 32 by 32 matrix. The axis of the matrix can be either the indices of the matrix or the physical values, this more useful for future interpretation. The shading of each cell corresponds to the count itself, which is the number of cycles that meet these values. The cycles counted are originally in *from-to* form, referring to the point *from* where each cycle starts and the point *to* where ends, see Figure 2.50.a From this basic representation, the max-min representation is obtained taking into account the similarity between those cycles starting in a maximum or in a minimum, but with the same range and mean. For example, two cycles (70,30) and (30,70) in a from-to representation, are count as two cycles of (70,30) in a max-min representation. Figure 2.50.b shows the max-min RFM. On the same way, the range-mean RFM (see Figure 2.50.c) is obtained by calculating the range and mean of each cycle from their maximum and minimum. Range-mean RFM is commonly used for fatigue applications. [22, p. 44-49]

A useful number to compare between different RFM is by their damage. The damage of a load is the well-known pseudo damage number:

$$d = \sum_i S_i^{\beta} \tag{2.20}$$

This number is obtained independent of the material model. The parameter S_i is the amplitude of each cycle counted, while the parameter β is the damage exponent, which reflects the type of component to be analyzed, having β=3 for welded components or crack growth, β=5 for typical automotive components with rough surface and β=7 for components with smooth surfaces. For this study, β=5 is going to be used.

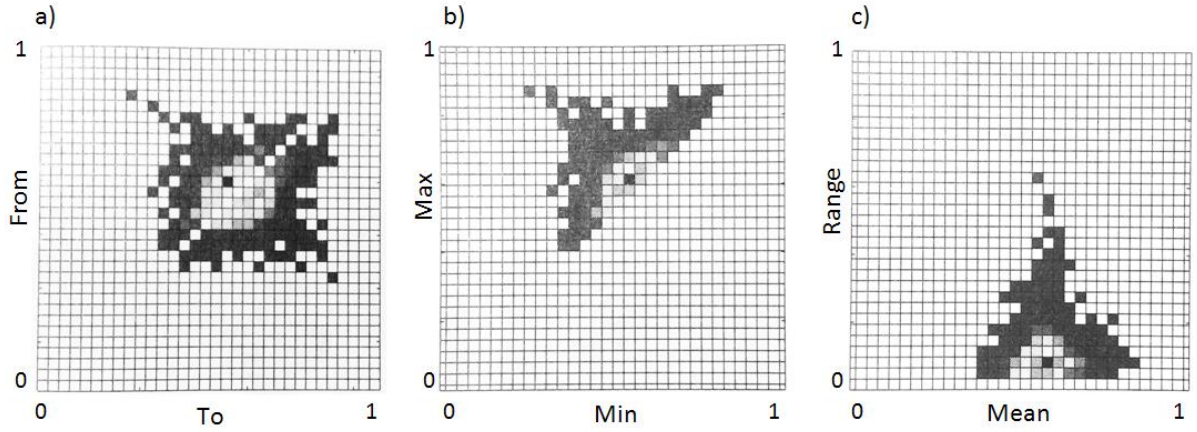

Figure 2.50: Different representation of the RFM. (a1) From-to RFM, (b1) Max-min RFM, (c1) Range-mean RFM [22, p. 49-50]

3 Simulation

3.1 SIMPACK

3.1.1 Functionality

SIMPACK is a general Multi-Body Simulation Software used to model the dynamic behavior of interconnected rigid or flexible bodies that are subjected to translational and rotational displacements. While single bodies or parts of a mechanical system are studied in detail with finite element methods, the behavior of the whole Multi-Body system is studied with Multi-Body System Methods.

It enables engineers to generate and solve virtual 3D models in order to predict and visualize motion, coupling forces and stresses. The main advantage of this software is that it is adapted to full transient non-linear analyses, even within the acoustic range, being particularly outstanding in transient high frequency analysis.

SIMPACK is particularly well suited for analyzing the dynamics of complex systems. [20]

3.1.2 Modelling Elements

- *Globals:* Time, Gravity, Search Path.
- *Solver Settings:* contains all settings for all SIMPACK solvers. Each model should contain at least one *Solver Settings* element, otherwise the solvers will use their internal default settings, which are unfavorable for most models.
- *SubVars (Substitution Variable)* are used for the parameterization of data. Instead of assigning the data explicitly a *SubVar* is assigned.
- *The Reference System* provides the basic coordinate frames for the model. The best-known is the general inertial system, Isys, which is stationary.
- *A Body* contains mass and inertia information and is kinematically connected to other bodies by means of *Joints*.
- *Markers* are used as connection points on bodies, as well as *Reference Systems*. Their position and orientation is defined relative to a Reference *Marker* that can be either the Body Reference Frame (default) or any other *Marker* on the *Body.*
  Marker 78 – Rail Wheel Profile Reference provides the reference systems for the rail and wheel profiles. It detects automatically whether it belongs to the rail or the wheel and which rail or wheel profile reference *Marker* is associated.
- *Primitives* provide the 3D graphical representation, for *Bodies* and also *Reference Systems*. There are various different types of *Primitive*, ranging from simple cuboids to

highly detailed and application specific types. *Primitive 21 – Wheel Rail Cab* (see Figure 3.1.a), *Primitive 22 – Wheel Rail Bogie* (See Figure 3.2), *Primitive 78 – RWC Wheel* (see Figure 3.1.b), *Primitive 79 – RWC Rail (*see Figure 3.1.c) are some examples of the *Primitives* most frequently used in railway modeling.

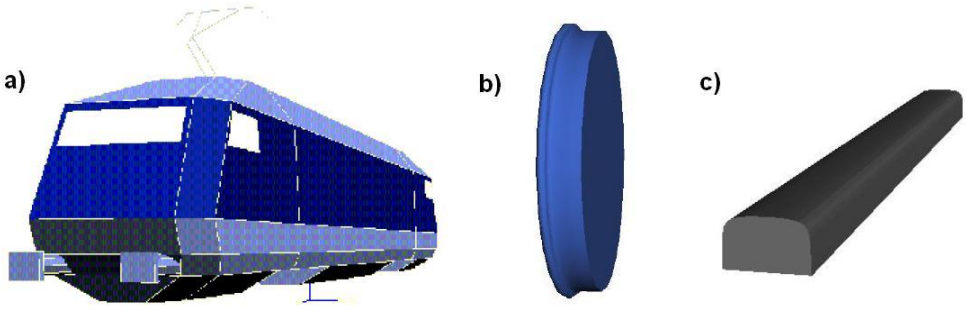

Figure 3.1: Primitives 21 (a), 78 (b) and 79 (c) [20]

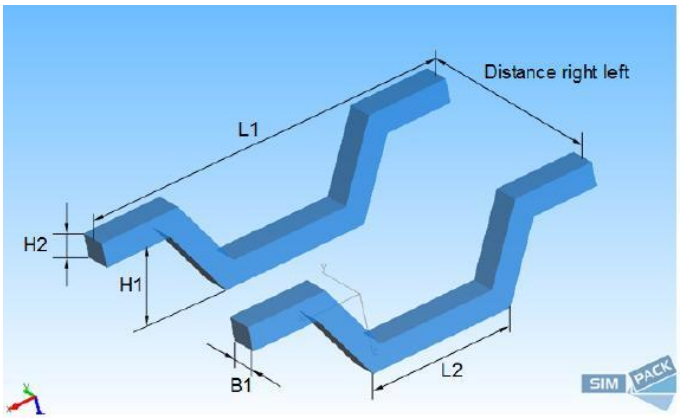

Figure 3.2: Primitive 22 [20]

- *Joints* define the relative motion between a *Body* and either the *Global Reference System (Isys)* or another *Body*. The type of *Joint* defines the degrees of freedom (DOF) that the *Body* has (0 to 6 DOF). The definition of the *Joint* serves to entirely describe the motion that the body may perform. *Joints 7 and 9*, the so-called Track *Joints*, are used for wheelsets, bogie/truck frames and carbodies, their degrees of freedom are related to the *Track.*

  Joint 7 describes the movement of the main components of a rail vehicle in space. It is typically used for the carbody, the bogie frames and the wheelsets.

  Joint 9 prescribes the movement of a rail vehicle component along a *Track* in space, prescribing a constant speed or a speed profile to a carbody of a rail vehicle or to a 'traction *Body*' for pushing or pulling a rail vehicle.
- *Constraints* are used for firmly joining *Markers* together. They are additional boundary conditions in the kinematics of the model.

- *Force Elements* are the standard choice for applying forces and torques of any kind to the model. *Force Element 78 – Rail Wheel Interface* provides the contact calculation between rail and wheel. It is not intended to be edited by the user; all parameters of the rail-wheel contact are controlled by the *Rail-Wheel Pair.*
- Rail-Wheel Pairs contain all information related to the rail-to-wheel contact and its geometry, *see* Figure 3.3 There must be one *Rail-Wheel Pair* for each wheel of a vehicle. Each *Rail-Wheel Pair* brings its own rail with it being possible that wheels run on totally different rail profiles.

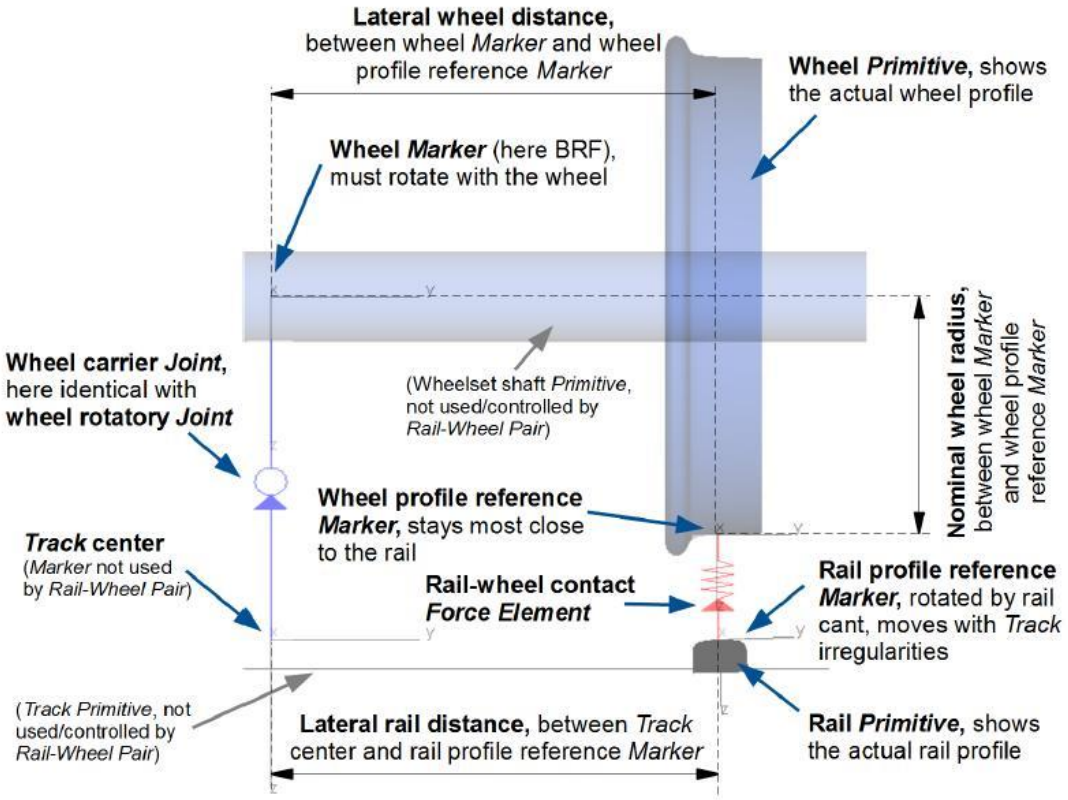

Figure 3.3: Geometrical wheelset definitions [20]

- *Rail-Wheel Contacts* define how the tangential forces and the tangential torque for the rail-wheel contact patches are calculated. There is a library of various tangential forces methods for engineering and scientific purposes.
- *Track Pairs* are passive Modeling Elements that provide a logical connection between a left-hand and a right-hand *Rail-Wheel Pair*, for example the two wheels of a wheelset. The use of *Track Pairs* is optional.
- *Tracks* define the layout and the irregularities of the track in the three-dimensional space. [20]

3.2 MATLAB

3.2.1 Functionality

MATLAB (MAtrix LABoratory) is a multi-paradigm numerical computing environment and fourth-generation programming language. It allows matrix manipulations, plotting of functions and data, implementation of algorithms, creation of user interfaces, and interfacing with programs written in other languages, including C, C++, Java, and Fortran. The MATLAB application is built around the MATLAB language. The general way to use it is typing MATLAB code into the Command Window (as an interactive mathematical shell), or executing text files containing MATLAB code, including scripts and/or functions.

3.2.2 Application to this work

Using MATLAB data files generated by SIMPACK (with the extension .m), the data are processed and new more useful graphs are generated.

The function generated in MATLAB (see ANNEX B for more details) has as input a load history data file previously generated by SIMPACK Post. These data are processed and transformed, applying the 4-Point Rainflow Algorithm, to obtain a final representation of the well-known Rainflow Matrix. This Rainflow Matrix obtained, shown in Figure is a form-to matrix, with the physical values as axis of the matrix. The pseudo damage number is shown in the title of the matrix, to make easier the comparison between matrixes.

3.2.3 Verification of the function

To justify the use of the function generated in Matlab along this work, the results obtained on it has to be proved by using a practical example. The example that is going to be used has been extracted from [22, pp. 44-45] and is also explained in Appendix B as example for the 4-point algorithm.

From an original load history, the cycles counted and the residual are extracted by applying the 4-point algorithm (see Figure 2.33). The explanation of the steps follow to obtain this information is described in Appendix B. Applying this algorithm to the load history in Figure 3.4, the result is the following:

$$\text{RFM} = [(7,4),(5,4),(2,6),(4,5)];\ \text{Residual: RES} = (2,8,1,7,2,5) \qquad (3.1)$$

From the cycles counted, a basic first representation of the rainflow matrix is done, as shown in Figure 3.5.a.

The pseudo damage number of the load under study can be obtained by applying the formula that defines this number:

$$d = \sum_i S_i^{\beta} \tag{3.2}$$

As explained in Section 2.6.4, the parameter S_i is the amplitude of each cycle counted, while the parameter β is the damage exponent, 5 for this study. Applying this formula to this example is obtained:

$$d = 3^5 + 1^5 + 4^5 + 1^5 = 243 + 1 + 1024 + 1 = 1{,}269 \cdot 10^3 \text{ kN}^5. \tag{3.3}$$

Figure 3.5.b. shows the result obtained using the Matlab function to the load under study. As can be see, the pseudo damage number obtained is the same as the one obtained bellow applying the formula. The matrix has a different representation of the one obtained before, but with same final results.

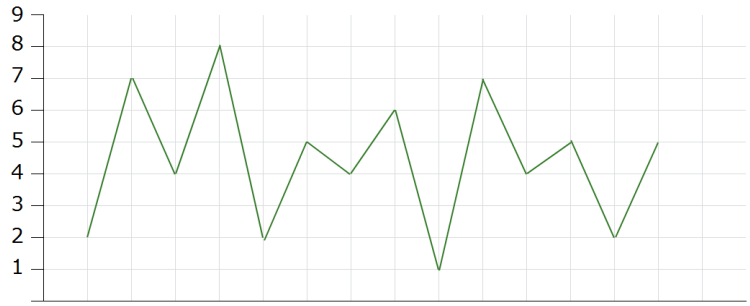

Figure 3.4: Load history under study

a)

from \ to	1	2	3	4	5	6	7
1	0	0	0	0	0	0	0
2	0	0	0	0	0	1	0
3	0	0	0	0	0	0	0
4	0	0	0	0	1	0	0
5	0	0	0	1	0	0	0
6	0	0	0	0	0	0	0
7	0	0	0	1	0	0	0

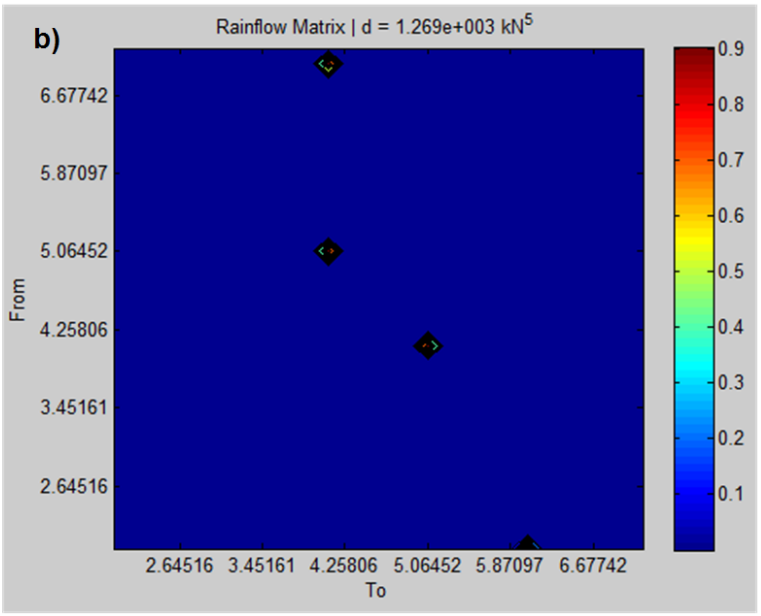

Figure 3.5: RFM obtained (a) by hand, (b) by the Matlab function

3.3 Modeling of Combino

As has been mentioned before, actual calculation of dynamic forces is extremely complex. In complex dynamic systems such as railway system, in order to understand its response to dynamic vehicle loading, two subsystems are first created: *vehicle subsystem model* and *track subsystem model*, between which there is a physical wheel/rail contact. Later on, a combination of these subsystems results in the entire system. [9, pp. 39-40; p. 47]

A model has to have sufficiently small simulation errors and, at the same time, be as simple as possible, to maximize computational efficiency. To minimize these errors, models are validated against real experimental data and, for that reason; the model has to be chosen according to each specific case. [10, p. 74]

Vehicle submodels may be represented either by Rigid or Elastic Multibody Models, depending on the frequency range. Rigid Multibody Models are appropriated in low frequency range while Elastic Multibody Models are useful to solve acoustic problems related to wheel resonance at high frequencies. [9, p. 47-49]

In this work, a Rigid Multibody Model of the Siemens tramway *Combino* has been developed using the software SIMPACK v.9. In the following sections, the configuration of the model is explained and illustrated. The joints, forces elements and couplings used within the model are represented in schematic diagrams. The joints are there represented in circles with the DOF referenced to the coordinate system shows in Figure 3.6, where x is the direction of movement of the tramway. On them, beside the type of joint, the displacement (x, y, z) and angular displacements (α, β, γ) that this joint allows and constrains are represented in green and red respectively, as shown in Figure 3.7. On the force elements representation, the number referring to the type of force element used is shown.

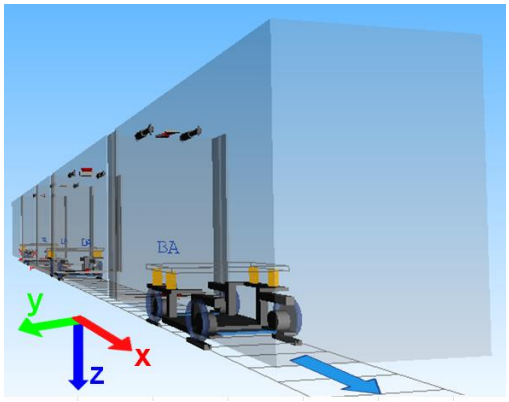

Figure 3.6:Coordinate System of the Model.

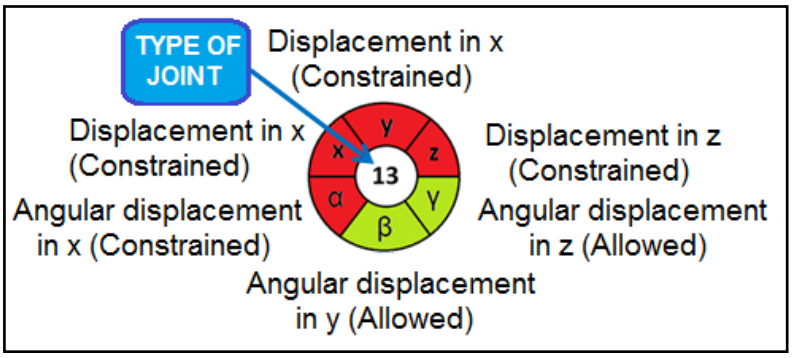

Figure 3.7: Joint schematic diagram example

3.3.1 Bogie Substructure

The *Bogie Substructure* has been modelled in a substructure compound, in turn, of three substructures: the *Frame* and two *Axles*. The main characteristics of the bogie are the primary and secondary suspensions. Primary suspension connects each *Axle Substructure* with the frame, while secondary suspension connects the *Frame* with the *Dummy* (both bodies of the *Frame Substructure*). All these components are shown in Figure 3.8.

Joints and Force Elements between bodies and Substructures within the Bogie Substructure and the Reference System are schematically represented in Figure 3.9. On it the primary suspension (between axle and frame) and secondary suspension (between frame and dummy) are shown. Axle and Frame are both connected to Isys with a Joint 7 allowing them the movement along the track. The wheels are attached to the axle with a Joint 2, which allow them only the rotational movement along y direction.

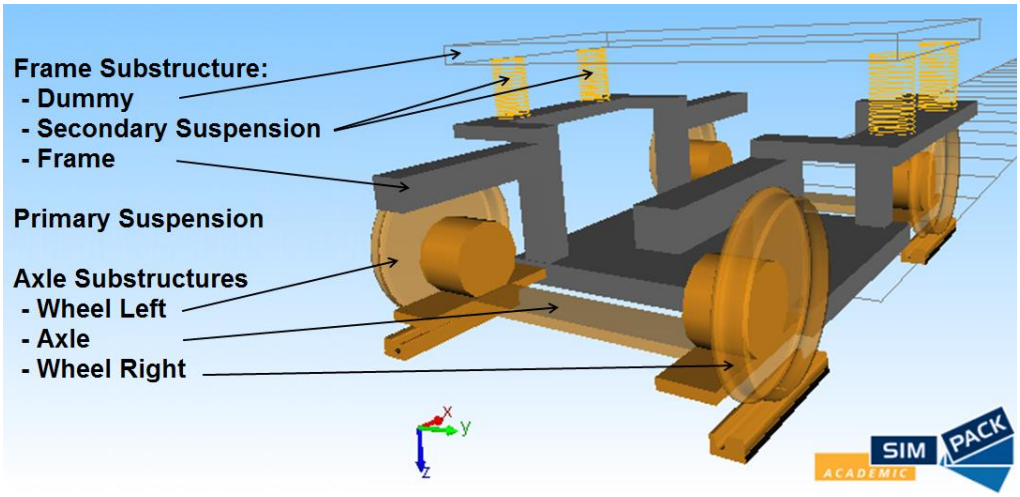

Figure 3.8: Frame and Axle Substructures within the Bogie Substructure

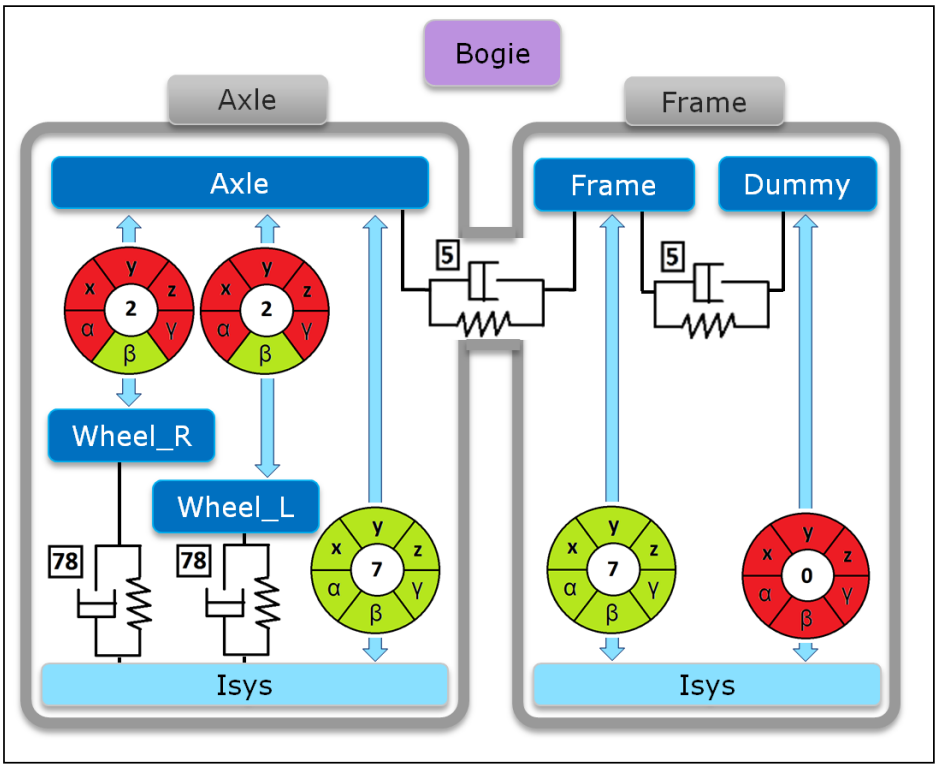

Figure 3.9: Bogie Substructure schematic diagram representation.

3.3.2 Articulations Substructures

There are two kinds of articulation substructures, one only regarding the z-direction and one regarding yz-directions. This is because of the specific need of z and y attachment between cars: z-direction is needed in each specific attachment and y direction is only needed once in the whole length of the vehicle. In our specific case, the YZ Articulation Substructure has been coupled in second position, in between the second and the third card. For more details see Section *3.3.3.*

The Z Articulation Substructure is divided in two parts: A and B, with a joint of 0 dof and the application of several force elements in between. This division is well-shown in Figure 3.10.

The Intercar Yaw Dampers are modelled in these substructures. This modelling is done by dividing the dampers in two parts. Each part is connected to one part of the *Articulation Substructure*, A and B, via a Joint that allows only the rotational movement in z direction (gamma γ), and are connected between them via a *Force Element*. These *Joint* and *Force Element* are shown in Figure 3.11.

Besides that, there are two more Force Element acting in the *Z Articulation Substructure*, and three more in the *YZ Articulation Substructure*. The corresponding to top and bottom,

shown in Figure 3.12, are common for both substructures, while the corresponding to the before explained y-direction damping attachment, shown in Figure 3.13, is exclusive for the *YZ Articulation Substructure.*

The *Joints* and *Force Elements* between Bodies within the *Z and YZ Articulation Substructures* and *Isys,* are schematically represented in Figure 3.15 and Figure 3.15.

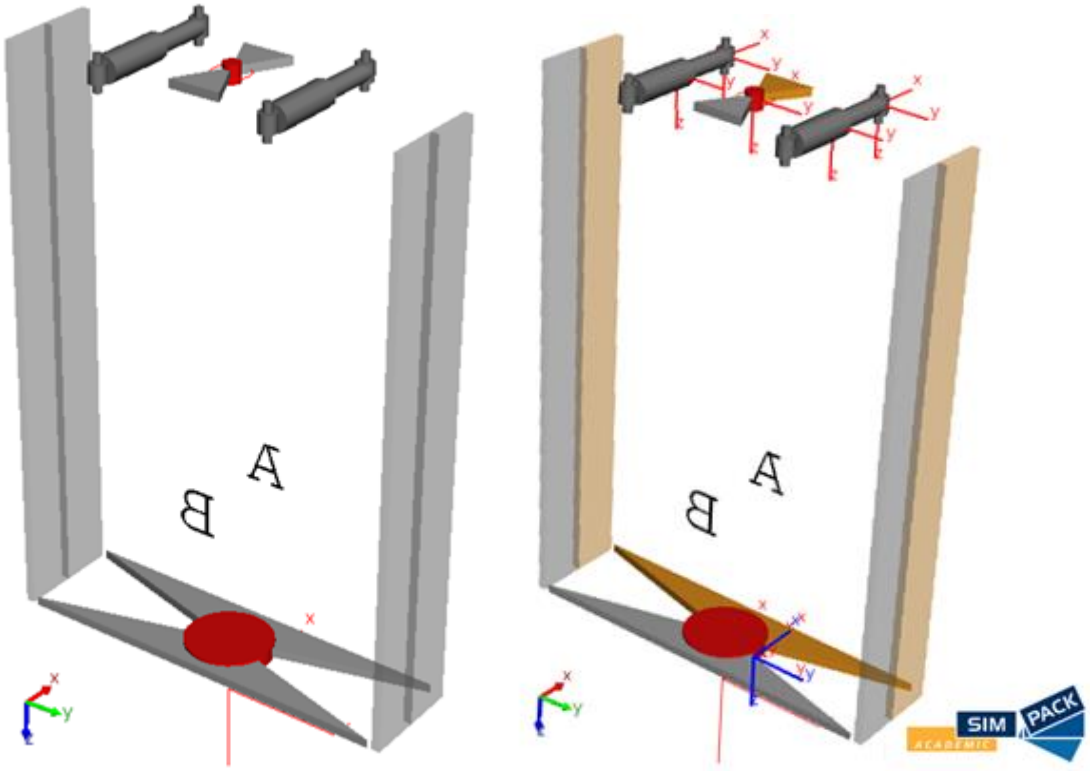

Figure 3.10: Parts A and B of the Z Articulation Substructure

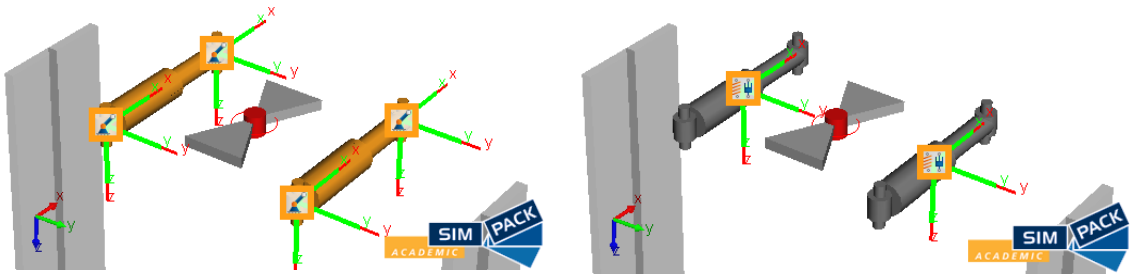

Figure 3.11: Intercar Yaw Damper configuration.

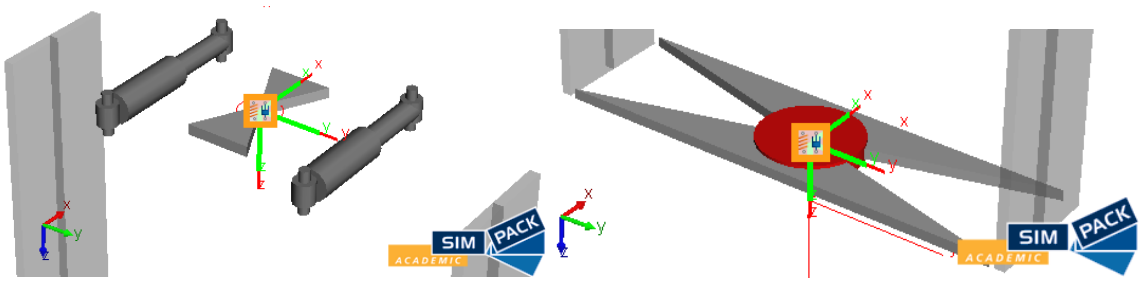

Figure 3.12: Top and bottom Force Elements. Z attachment.

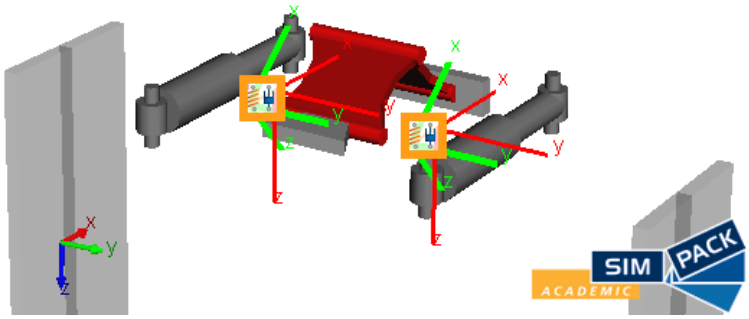

Figure 3.13: Top Force Element. Y attachment.

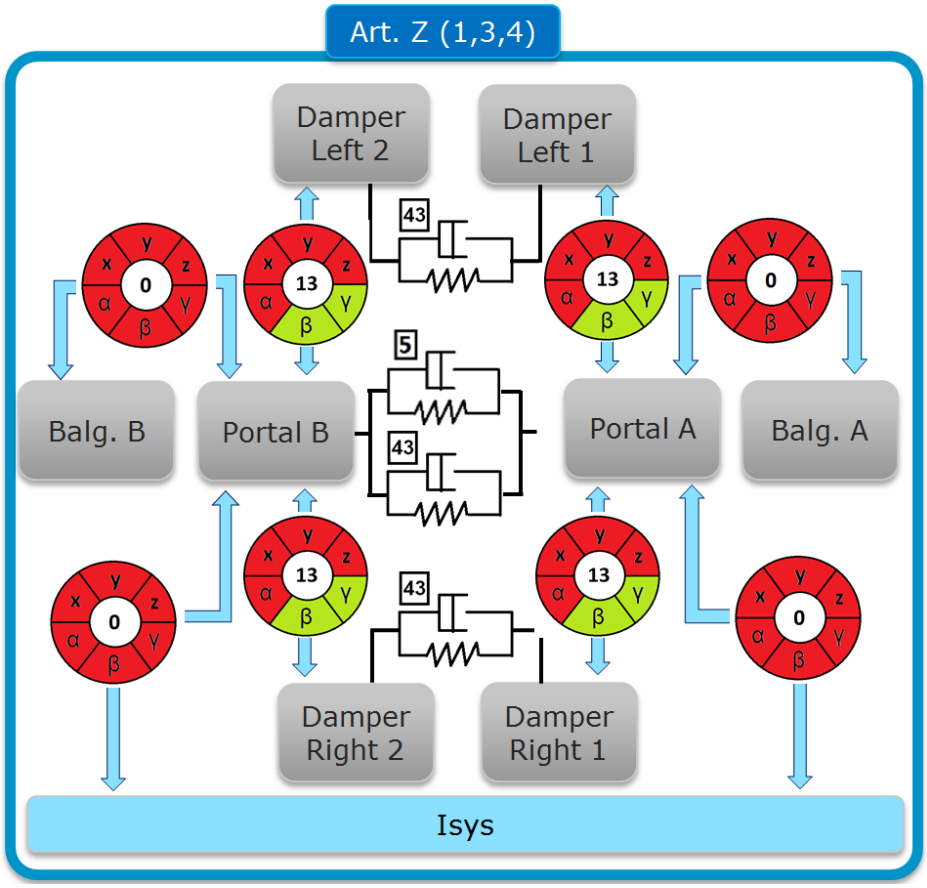

Figure 3.14: Z Articulation Substructure schematic diagram representation.

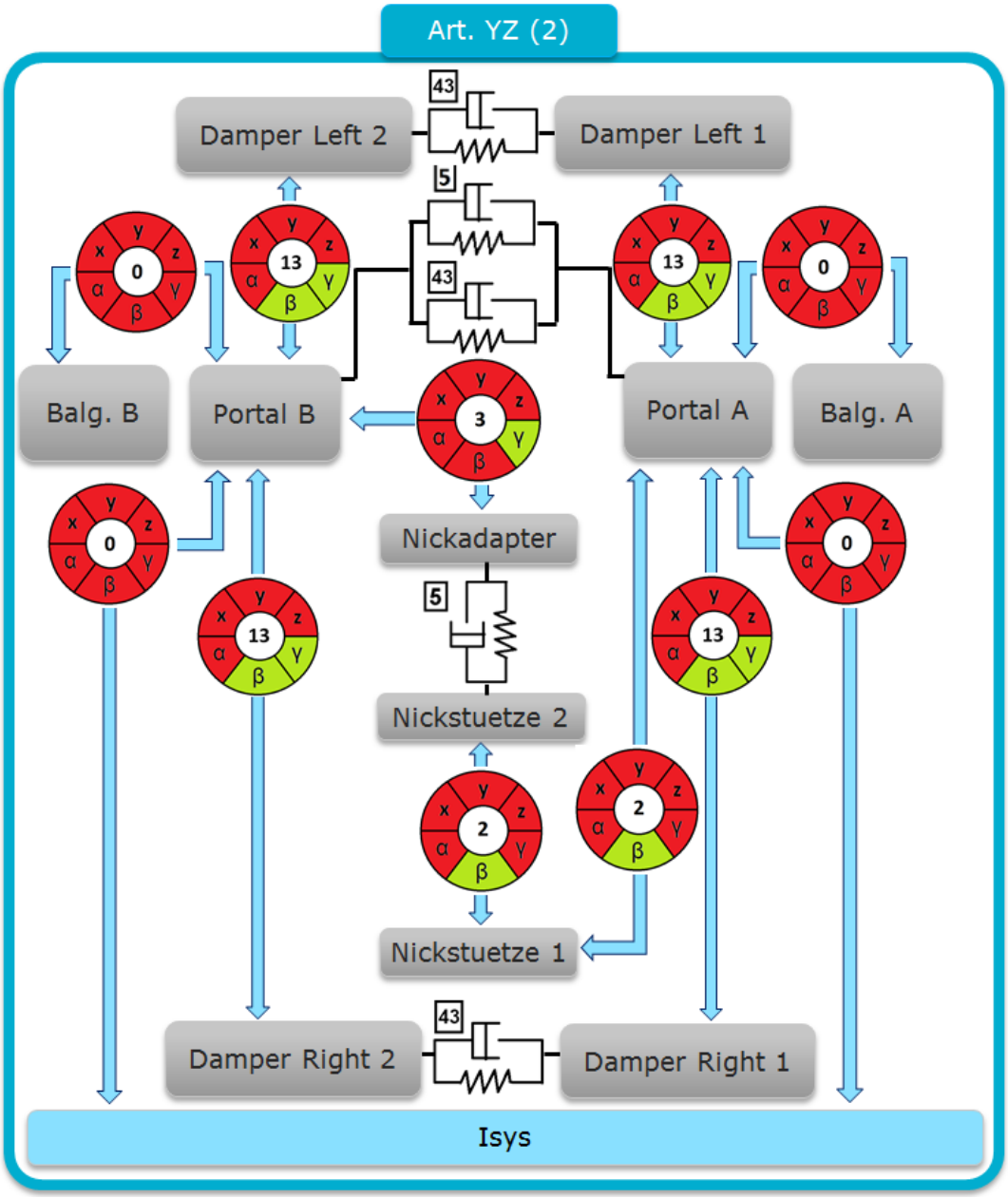

Figure 3.15: YZ Articulation Substructure schematic diagram representation.

3.3.3 Main model

Figure 3.16: Perspective view of the Main model

The Main model (Figure 3.16) is compound by twelve substructures, shown in Figure 3.17: five *Car Substructures* (formed by a simple cuboid body, with all its parameters related to its length, which changes from one car to the other.), three *Z Articulation Substructures*, one *YZ Articulation Substructure* and three *Bogie Substructures.*

Although at first sight the model looks geometrically symmetric in the z-y plane, there are two important differences:

- All the *Car Substructures* have Joint 7 (General Rail Track Joint) to Isys, with the exception of the first car, which has Joint 9 (Rheonomic Rail Track Joint). This is to achieve a constant velocity during the rolling of the vehicle.
- As mentioned before, the second articulation is a *YZ Articulation Substructure.*

The *Joints* and *Force Elements* between the twelve structures and the *Reference System* (*Isys*) are schematically represented in Figure 3.18.

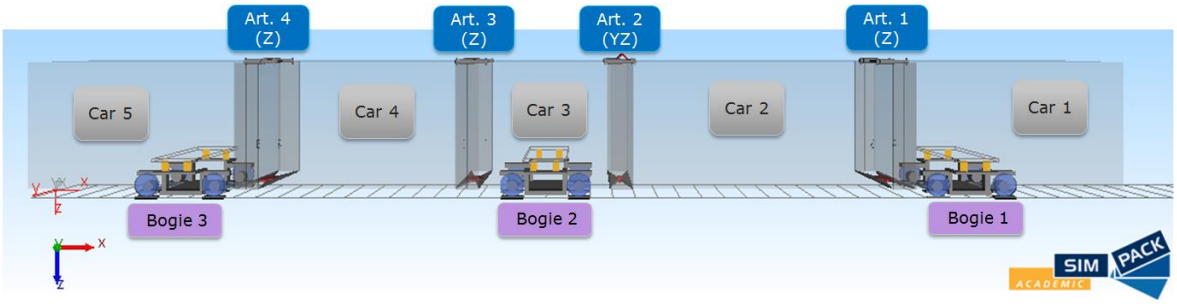

Figure 3.17: Substructures that composed the Main model

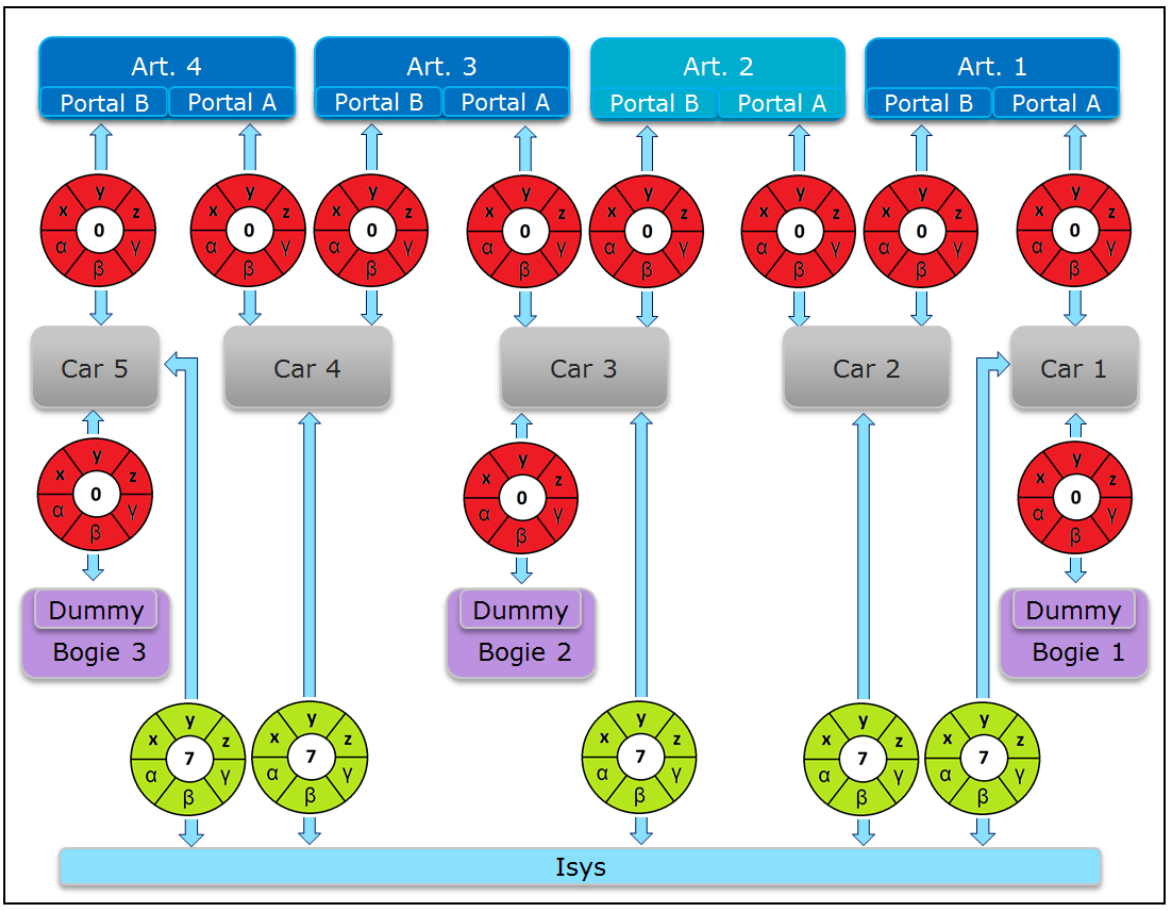

Figure 3.18: Main model schematic diagram representation.

3.4 Simulation scenarios

Several scenarios (see Table 7) and results obtained from these scenarios (see Table 8) have been simulated and extracted from the model previously described using SIMPACK v.9. Following, each result will be explained supported by some example graphs of it. The excitations applied to the model are those defined by Frederich. In Figure 3.19 can be appreciated the increase of severity of the excitations from good to bad.

Table 7: Scenarios simulated

Scenario	Velocity	Track	Excitation	Time	Comments
0	70 km/h	Straight	FRED_bad	30 s	Without yaw damping
1	35 km/h	Straight	FRED_bad	30 s	-
2	70 km/h	Straight	FRED_bad	30 s	-
3	35 km/h	Straight	FRED_MiddleBad	30 s	-
4	70 km/h	Straight	FRED_MiddleBad	30 s	-
5	35 km/h	Straight	FRED_Good	30 s	-
6	70 km/h	Straight	FRED_Good	30 s	-

Table 8: Results obtained

Results	Description	Scenarios to apply	Total number of graphs
A	Angular displacement of left and right yaw dampers related to the center of the articulation.	2 (Last car)	1
B	Comparison of angular position (gamma) between two consecutive cars for second and last articulation.	0, 2 (1^{st} and 2^{nd} cars)	2
C	Lateral displacement of each axle related to the lateral excitation.	1-6	36
D	Yaw damper forces in x direction (2^{nd} and last articulations)	1-6	12
E	Reaction forces (F_x and $F_{y)}$ in the last carbody.	1-6	6

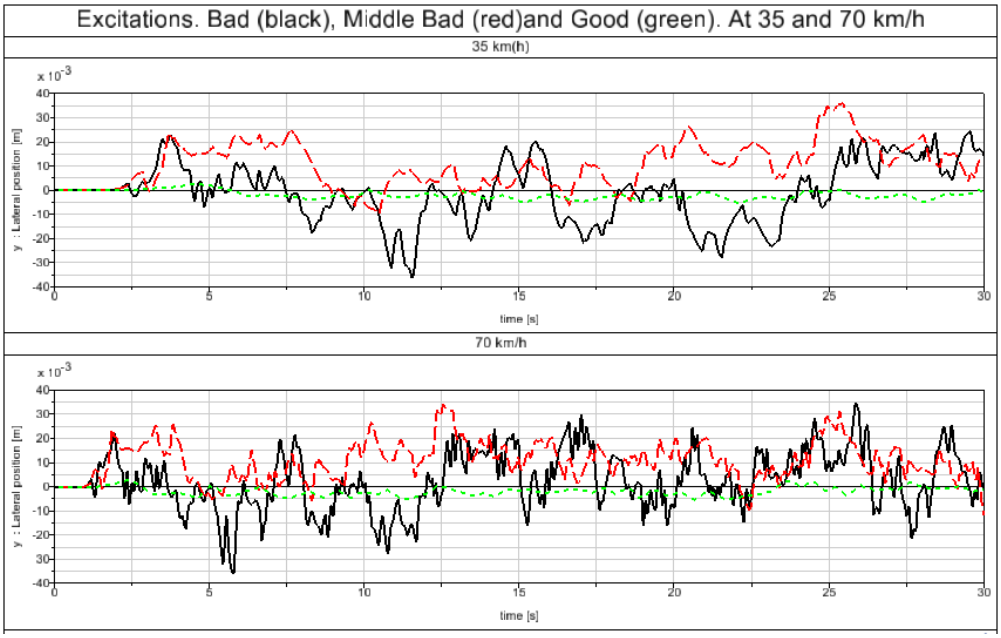

Figure 3.19: Excitations applied to the model.

The first study (A of Table 8) has been achieved to prove the parallelism of both yaw dampers of the same articulation along the movement of the vehicle. As shown in Figure 3.20 the angular displacement of each damper compared to the center of the articulation is approximately equal, for that reason, in next studies of yaw dampers it is only needed to check the result in one side, either left or right. It is needed to mentioned, that this approximation is only valid for yaw damper studies (D and E of Table 8).

To prove the Multi-body articulated vehicles behavior mentioned in Section 2.4, a comparison of the first and last carbodies has been done in B. The comparison is done via the angular displacement of the second and last car related to the previous car (first and forth).

This behavior is easily noticed when there is not yaw damping acting on the vehicle. In Figure 3.21 it can be appreciated that the angular position gamma is higher for the last than for the second carbody. These results represent the increase of the yaw movement oscillation along the length of the vehicle. The graphs for the same scenario with yaw damping (see Figure 3.22) have been also extracted, but this behavior is hard to prove for this case.

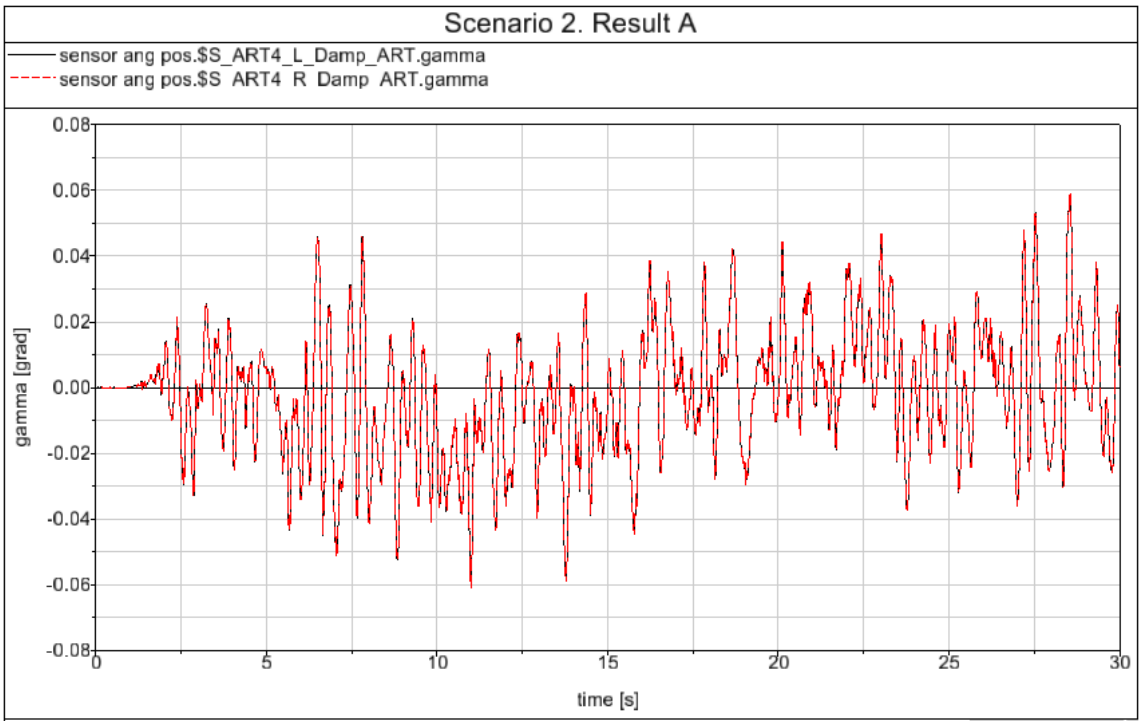

Figure 3.20:Angular displacement (alpha, beta and gamma) of left and right dampers compared to the center of the articulation

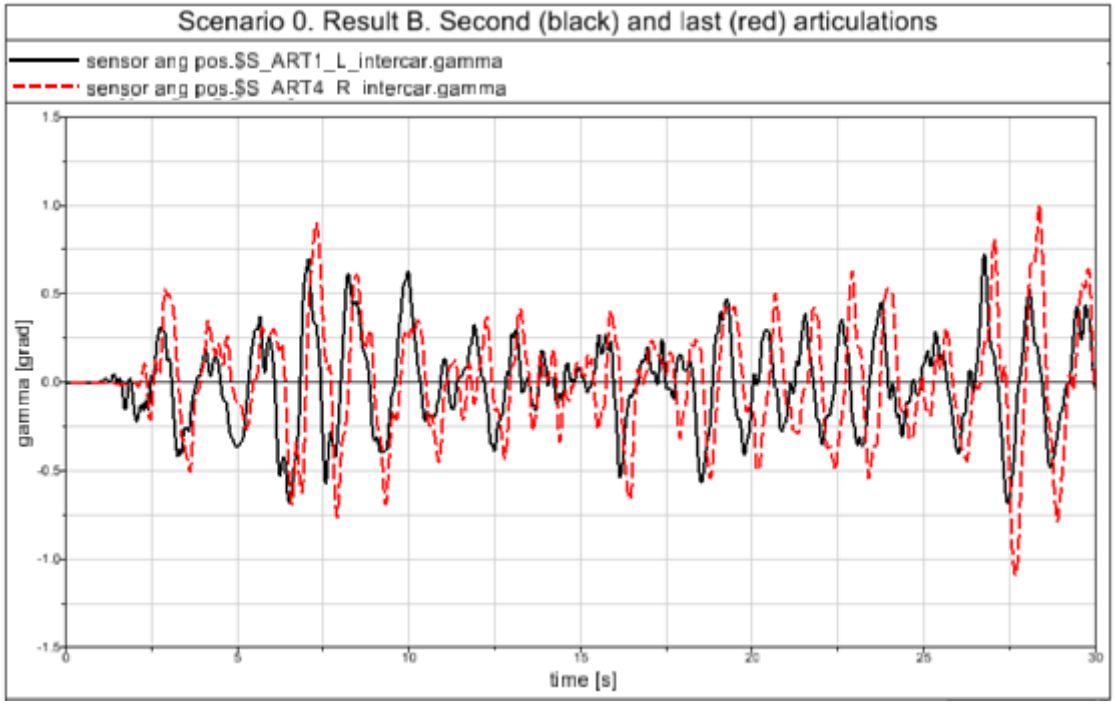

Figure 3.21: Comparison of angular position (gamma) between two consecutive cars for second and last articulation in scenario 0.

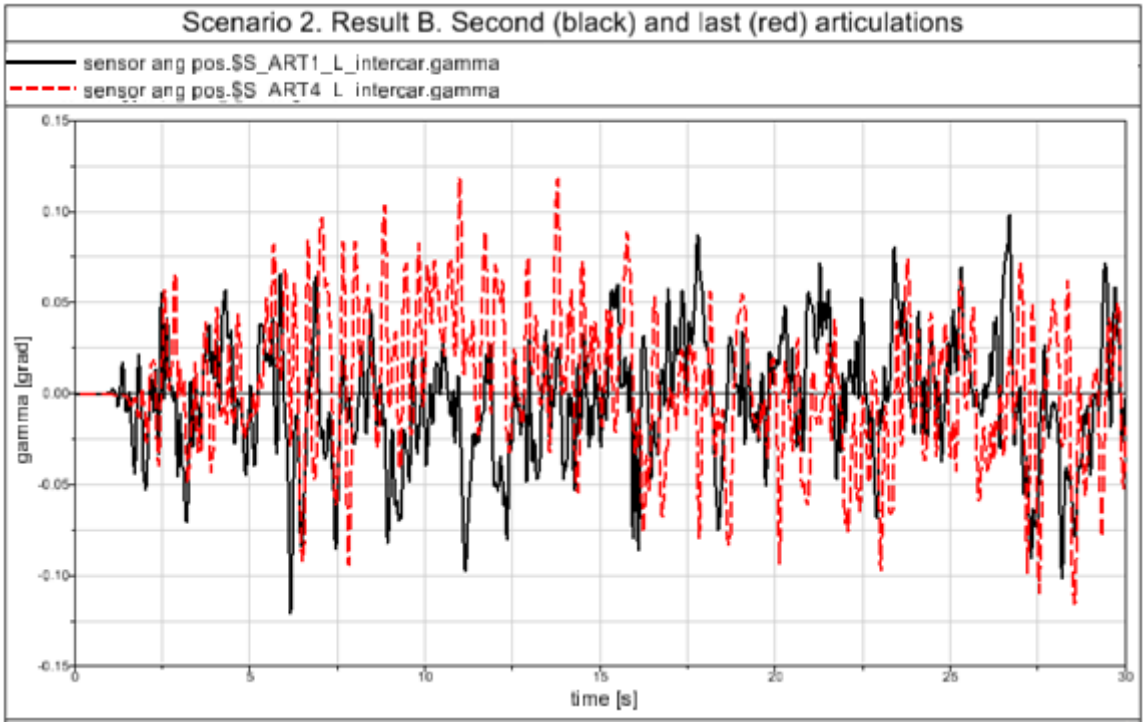

Figure 3.22: Comparison of angular position (gamma) between two consecutive cars for second and last articulation in scenario 2.

Once these facts have been checked and proved, the main study of the scenarios 1-6 can be done. These results are C, D and E of Table 8.

In C, one graph is extracted per axle and scenario; with six axles per scenario and six scenarios, 36 graphs are obtained in total. These graphs represent the lateral displacement of each side of the axle (lateral displacement of left and right wheel) related to the lateral excitation of the track. Their show the possible risk of derailment; when the lateral displacement of the wheel is close to the lateral displacement of the track (lateral excitation), the risk of derailment is bigger. Derailment will occur when the curve for the excitation surpass one of the curves for lateral wheel displacement. Some examples of these graphs are shown in Figure 3.23 and Figure 3.24.

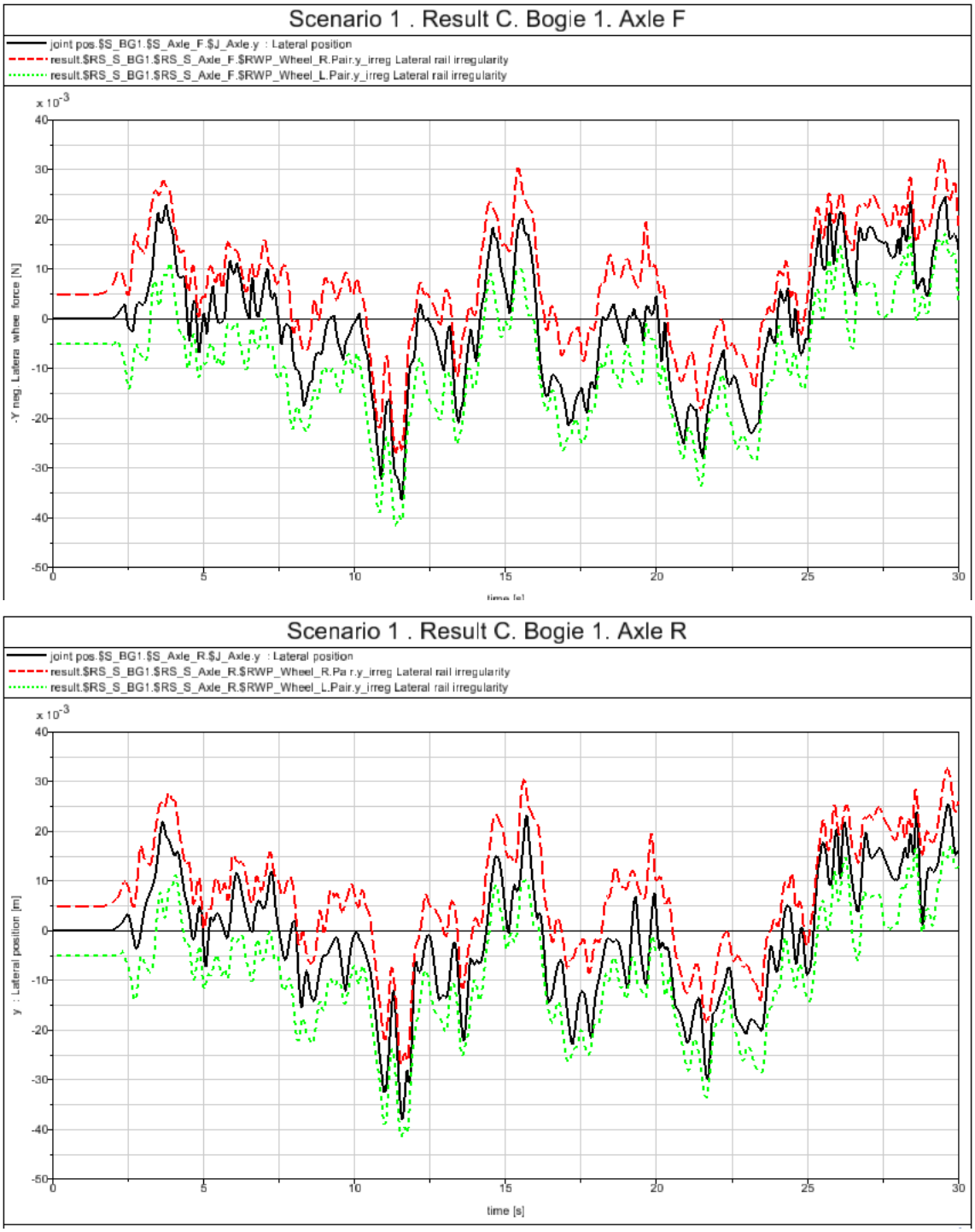

Figure 3.23: Lateral displacement of the right (red line) and left (green line) wheels with respect to the lateral excitation (black line) for first and second axle (first bogie) in Scenario 1.

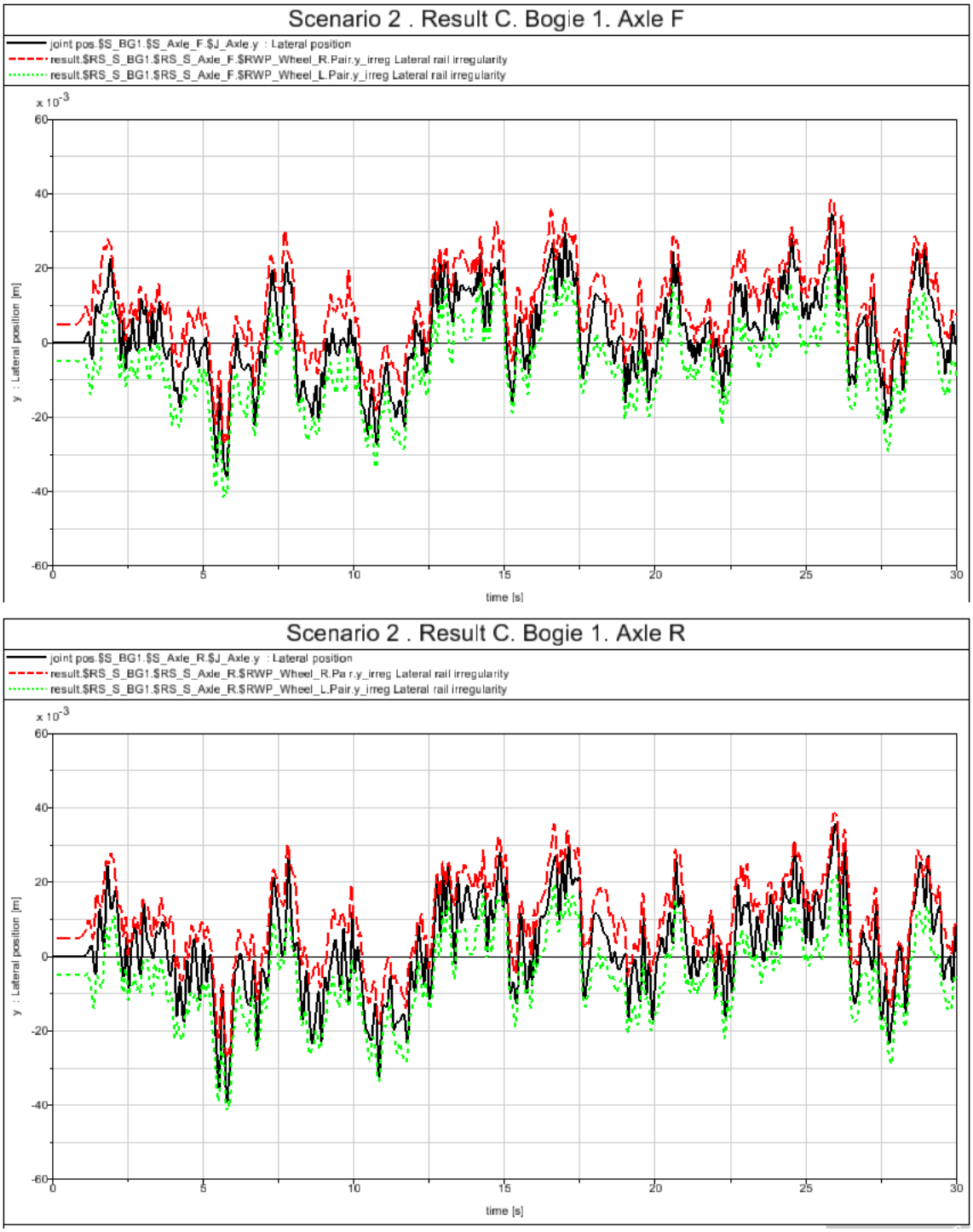

Figure 3.24: Lateral displacement of the right (red line) and left (green line) wheels with respect to the lateral excitation (black line) for first and second axle (first bogie) in Scenario 2.

In D, graphs of the yaw damper forces are obtained. Two factors are taken into account to decide which graphs are more important to analyze. The second articulation, as explained in Section 3.3.2, is the only one that damps the force in y and z directions and, as explained before, the most critical yaw movement takes place in the last car. For that reason, graphs of the second and last yaw dampers are extracted.

Graphs in E are extracted by multiplying the graphs in D (yaw damper forces in x direction) by the sine and cosine of the angular displacement in z direction (gamma) in between the coordinate system of the yaw damper and the coordinate system of the carbody along the movement of the vehicle. In Figure 3.25 both coordinate system and the angular displacement in between them are shown; the coordinate system of the carbody is represented in red, while the corresponded to the yaw dampers is represented in blue. The transformation of coordinate system is also represented in Figure 3.25 , the Yaw Damper force (in blue in the left draw) is reflected in a reaction force in the carbody (in red in the right draw) that it is, on its way, reflected in two forces in the carbody coordinate system, one in x direction F_x and another in y direction F_y (in brown in the right draw). F_x is obtained by multiplying the original force by the sine of the angle gamma, while F_y is obtained multiplying it by the cosine of the angle gamma.

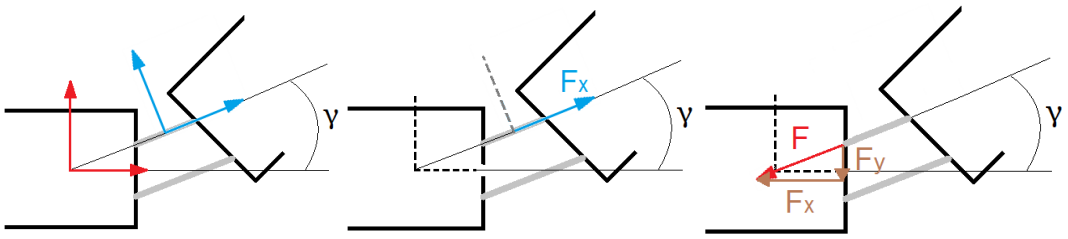

Figure 3.25: Representation of the angular displacement (gamma) between yaw damper (blue) and carbody (red) coordinate systems, the yaw damper force (blue), the reaction force associated (red) and the reaction force components F_x and F_y (brown)

In that way, as shown in Figure 3.26, two graphs of the reaction in the carbody are obtained per graph of yaw damper force, one in x and another in y directions of the carbody coordinate system. As the angle gamma is very low (in the order of 10^{-3} rad), the graph obtained for the sine of it is approximately the angle itself, and the cosine of it is around 1.

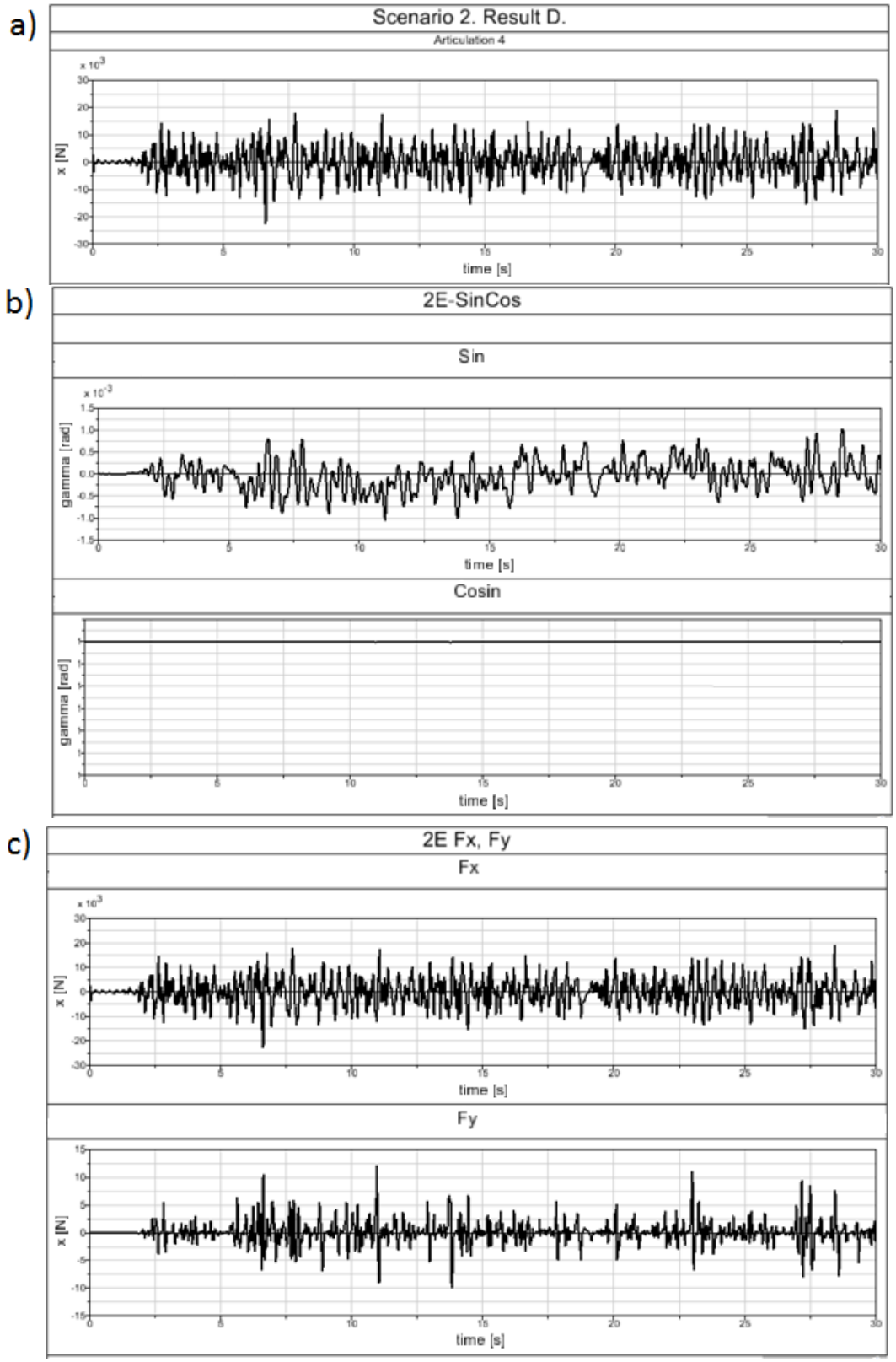

Figure 3.26: Example of obtaining graphs for E in Scenario 2.
(a) Original Yaw damper force, (b) Sine and cosine of the angle gamma. (c)Two reaction forces F_x and F_y result of the yaw damper force.

To understand better the fatigue damaged of the forces, the Rainflow Matrixes of some graphs (1-6 D and 1-6E) are obtained and analyzed. The obtaining of the RFM is done by using the Matlab function explained in Section 3.1.2 and Appendix B.

Figure 3.27 shows some examples of the RFM of yaw damper forces of the last articulation in some of the scenarios under study. The diagonal virtual line crossing from the left-bottom point to the right-upper point on the graph is followed in all the cases. This line represents the cycles with a from-point similar to the to-point, which means that the amplitude of the cycle is small. The deviation from the center of the graph is due to an offset of this cycle with respect to zero. The pseudo damage number obtained in all the cases is compared in Table 9.

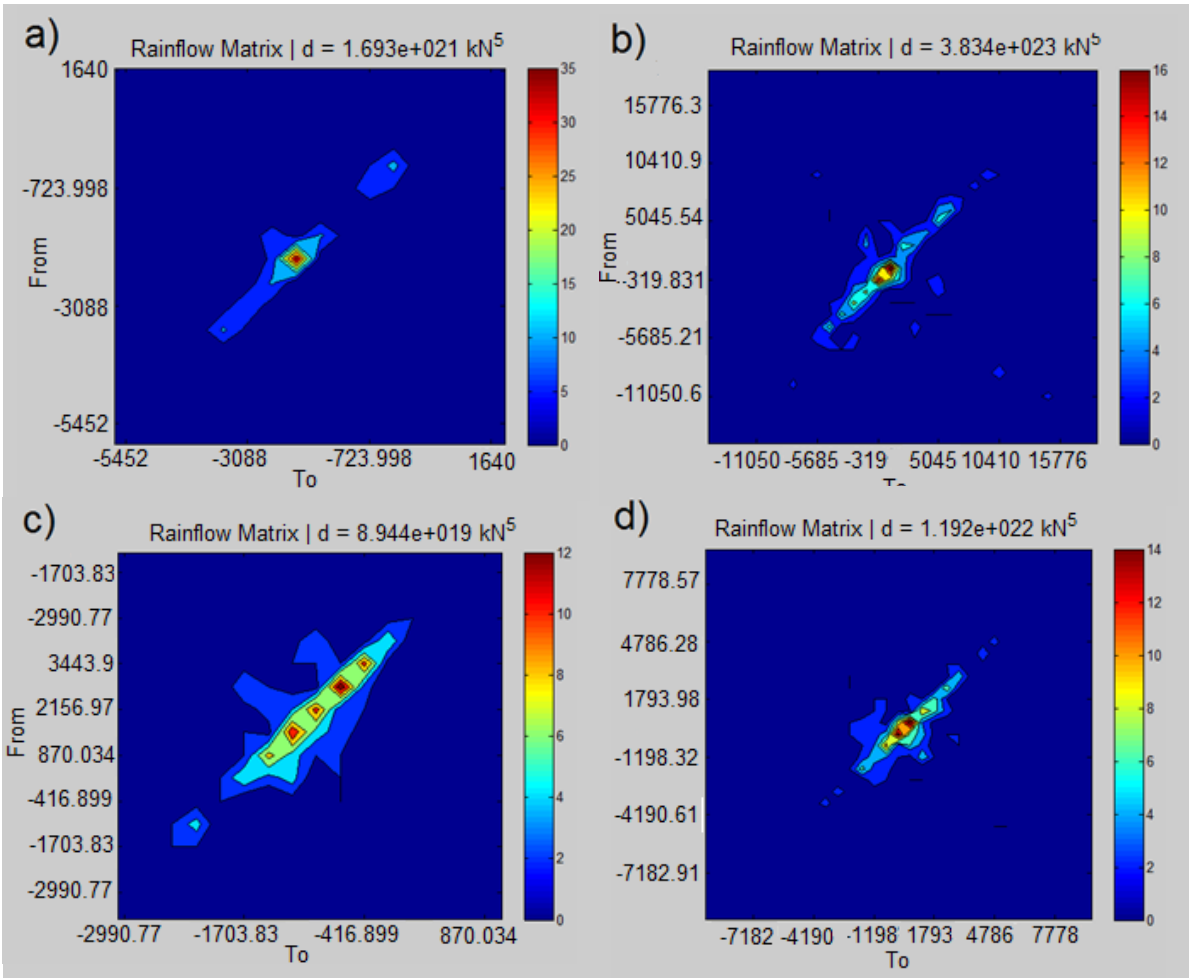

Figure 3.27: RFM obtained for the yaw damper forces in the last articulation for different scenarios: (a)1D, (b) 2D, (c) 3D, (d) 4D, (e) 5D, (f) 6D

Table 9: Pseudo damage number obtained for different results and scenarios.

Scenario	Velocity	Excitation	Pseudo damage number	
1D	35 km/h	FRED_bad	D	$1{,}693 \cdot 10^{21}$ kN^5
			E, F_x	$1{,}693 \cdot 10^{21}$ kN^5
			E, F_y	$1{,}366 \cdot 10^{4}$ kN^5
2D	70 km/h	FRED_bad	D	$3{,}834 \cdot 10^{23}$ kN^5
			E, F_x	$3{,}834 \cdot 10^{23}$ kN^5
			E, F_y	$4{,}737 \cdot 10^{6}$ kN^5
3D	35 km/h	FRED_MiddleBad	D	$8{,}944 \cdot 10^{19}$ kN^5
			E, F_x	$8{,}944 \cdot 10^{19}$ kN^5
			E, F_y	$1{,}953 \cdot 10^{1}$ kN^5
4D	70 km/h	FRED_MiddleBad	D	$1{,}192 \cdot 10^{22}$ kN^5
			E, F_x	$1{,}192 \cdot 10^{22}$ kN^5
			E, F_y	$2{,}396 \cdot 10^{4}$ kN^5
5D	35 km/h	FRED_Good	D	$5{,}832 \cdot 10^{16}$ kN^5
			E, F_x	$5{,}832 \cdot 10^{16}$ kN^5
			E, F_y	$7{,}748 \cdot 10^{-6}$ kN^5
6D	70 km/h	FRED_Good	D	$9{,}57 \cdot 10^{16}$ kN^5
			E, F_x	$9{,}57 \cdot 10^{16}$ kN^5
			E, F_y	$9{,}110 \cdot 10^{-5}$ kN^5

The results obtained in all the cases are compared in logarithm scale in Figure 3.28. There we can see how this damage is increasing when the rail excitation is getting worst and also when the speed of the vehicle is increasing. For the pseudo damage number obtained for results E, it can be mentioned that, as the angular displacement gamma is always very small, the reaction forces in x direction are approximately the same as the forces in the yaw dampers and, for the same reason, the pseudo damage associated to both are also the same. This fact is also the reason why the reaction forces in y and the pseudo damage number associated to them is very small. But this does not mean that it should not be taken into account. Though this number is not associated with the material properties, the fatigue damage is. The material properties are, in general much better in the x direction (direction of application of the loads) than in y direction and, therefore, the fatigue strength is also smaller in y than in y direction.

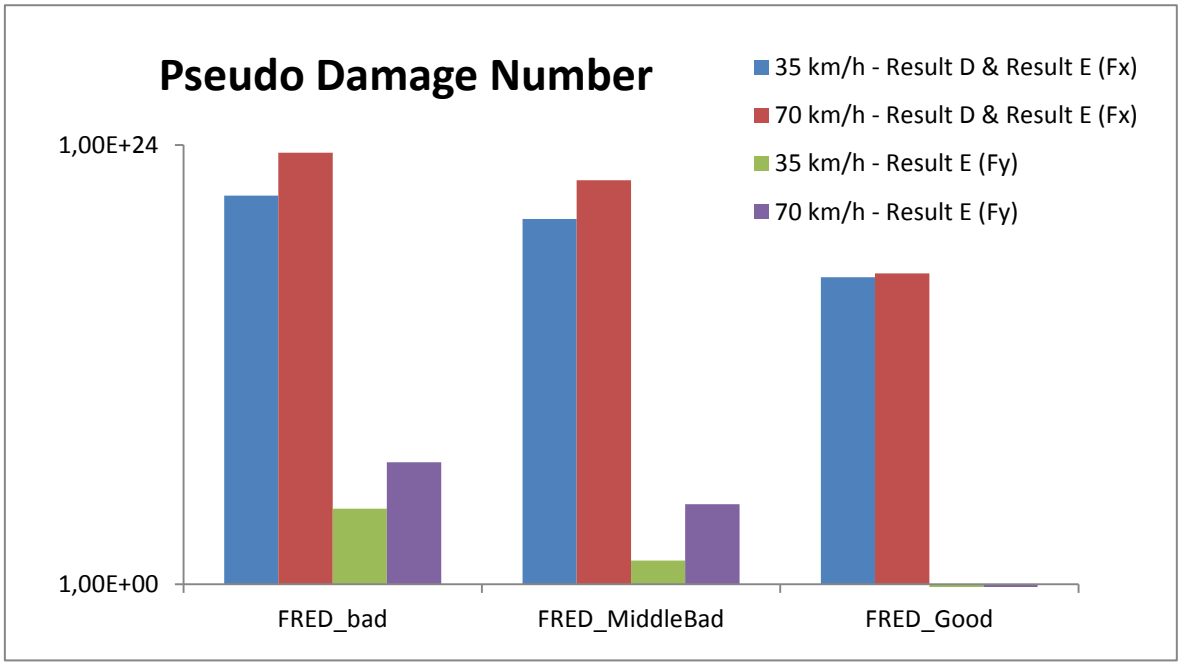

Figure 3.28: Comparison of the pseudo damage numbers obtained

4 Analysis

Several results have been obtained along the scenarios simulated within this work. Before start analyzing these results, it has to be mentioned that both Simpack model and Matlab function used along this work have been verified with examples before the study was started. The first instance of proving the Simpack Model was comparing the yaw damper forces obtaining on it with the approximate values, which were previously known. Later on, its functionality is also proved within the proper results obtained. On its own, the Matlab function has been proved by analyzing a practical example explained by JOHANNESSON P. and SPECKERT M. [21].

As mentioned before, the results of the post-simulation analysis of Simpack are first obtained to prove the theoretically known behavior for multi-articulated tramways. First of all, it has been verified, that each yaw damper (right and left) within the same articulation have an equal angular displacement with respect to the middle point of the articulation. With this it is proved that the different elongation of the dampers, affecting directly on the forces generated on them, is only a result of the angular displacement between the two wagons. The second result obtained for this goal is the lateral displacement of the last wagon in comparison to the first one. This result shows that this displacement is higher for the last wagon than for the first one, a well-known behavior of all the multi-articulated vehicles.

From that point, new results have been extracted from the model. The goal is to know the reaction better when running under different rail excitations and vehicle velocity scenarios, and the consequences of these reactions. The main results studied are the yaw damper forces and the consequent reaction forces generated on the wagon. In order to compare these results easily, the pseudo damage number has been used. This number has been obtained for all the cases within the Matlab function. This has been done taking in consideration the Hysteresis cycles of the load and, for that reason, with a direct relation with the fatigue damage evaluation. It has been seen that the rail excitation, affecting the vehicle as environment, has a direct impact in the fatigue life of it. The fatigue damage is increasing when increasing the velocity of the vehicle and also when running under worst excitation of the rail. The pseudo damage number obtained when running “slow” under “good” rail excitations is 6,5 million times the one obtained when these conditions are “fast” and “bad” excitation of the rail. But, how much is this number affected of the vehicle velocity? For same velocity, comparing “bad” and “good” rail excitations, the difference is 4 million times when running “fast” and 0,02 million times when running “slow”. While comparing “slow” and “fast” the difference is 200 times when running under “bad” rail

excitations and of 1,6 times when running under “good” rail excitations. The conclusion under these results is that the impact that the rail excitations got on the fatigue life has more weight than the impact that the velocity got on it. For that reason, the environment under which the vehicle is running has to be deeply analyzed to do a fatigue damage study of the vehicle.

5 Outlook

The tramway COMBINO of Siemens with five sections configured to run in Amsterdam has been developed for this work. On it, some studies have been done mainly focused on the yaw dampers and the last wagon behavior, confirming the behavior of the whole model. For that reason, in future studies, the same model could be used for different studies of the dynamic properties of the tramway, as could be its behavior when running through curves, slopes, steep curves, etc.

Along the work, a Matlab function has been verified and used. On this function, a Rainflow Cycle Counting is applied to an entered load history. The outputs of the function are the Rainflow Matrix and the pseudo damage number associated to the cycles extracted on it. For future load analysis to study the fatigue damage and durability of vehicles, the results obtained from this function would be of high importance. The reason of it is that the cycles extracted from the algorithm are those that are hysteresis cycles related.

As was explained in the analysis, the severity of the excitations of the rail has a big impact on the fatigue life of the vehicle. For that reason, in future studies of the fatigue damage, the characteristics of these excitations have to be deeply analyzed before start the fatigue damage analysis.

Bibliography

[1] ORLOVA, A., BORONENKO Y.: The Anatomy of Railway Vehicle Running Gear, Handbook of Railway Vehicle Dynamics, by Taylor & Francis Group, LLC, 2006

[2] KOCH, M.: URL http://www.spurkranzschmieranlage.de/lang1/technical_field.html, Gotha 2011

[3] SKF: Railway Technical Handbook, Vol. 2, 24-41, 2011

[4] THOMPSON, D.: Railway Noise and Vibration, Mechanisms, Modelling and Means of Control, 2009.

[5] ORTERO, Y. J.: Study of Tail Vehicle Dynamics in Curved Tracks. Part I: Wheel-Rail Contact Analysis, Revista Colombiana de Tecnología Avanzada, Vol.2, Num.14, 2009.

[6] FREDERICH, A. F.: Die Gleislage – aus fahrzeugtechnischer Sicht, Georg Siemens Verlagsbuchhandlung, 1984

[7] ABOOD, A. K. H., KHAN, R. A.: Hunting Phenomenon Study of Railway Conventional Truck on Tangent Tracks due to Change in Rail Wheel Geometry, Journal of Engineering Science and Technology Vol. 6, No. 2, 146 – 160, School of Engineering, Taylor's University, 2011

[8] CANO, E.: La seguridad en la marcha de los trenes y el movimiento de lazo, c3T, Universidad Tecnológica Nacional, Centro Tecnológico de Transporte, Tránsito y Seguridad Vial, 2010

[9] MARTYN, S. D.: Identification and Development of a Model of Railway Track Dynamic Behaviour, Thesis, Queensland University of Technology, 2005

[10] OSCARSSON J., DAHLBERG T.: Dynamic Train/Track/Ballast Interaction - Computer Models and Full-Scale Experiments, Vehicle System Dynamics: International Journal of Vehicle Mechanics and Mobility, 29:S1, 73-84, 1998

[11] ČAPEK J., KOLÁR J.: Optimal Design of Low-Floor Tram, From horse-drawn railway to high-speed transportation system, Czech Technical University in Prague, 2007

[12] SCHINDLER, C.: 20 Jahre Niederflurbahnen. Welche Konzepte setzen sich durch, Systemanalyse von Niederflur-Straßenbahnkonzepten, Der Nahverkehr, Technik, 2007

[13] SCHINDLER, C.: Grundlagen der Niederflurtechnik, Probleme und Lösungen beim Straßenbahn-Fahrzeugbau: Eine systematische Analyse, Der Nahverkehr, Technik, 2007

[14] SIEMENS A, siemens.com/mobility: Tram System - ULF Vienna, Austria, 2013

[15] BRUNI, S., RESTA, F.: Active control of railway vehicles to avoid hunting instability, IEE/ASME International Conference on Advanced Intelligent Mechatronics Proceedings, Como, Italy, 2001

[16] ALONSO, A., GIMÉNEZ, J. G., GOMEZ, E.: Yaw damper modelling and its influence on railway dynamic stability, Vehicle System Dynamics: International Journal of Vehicle Mechanics and Mobility, 49:9, 1367-1387, 2011

[17] BRAGHIN, F., BRUNI, S., RESTA, F.: Active yaw damper for the improvement of railway vehicle stability and curving performances: simulations and experimental results, Vehicle System Dynamics Vol. 44, No. 11, 857–869, 2006

[18] ORVNÄS, A.: Active Secondary Suspension in Trains, Royal Institute of Technology, Aeronautical and Vehicle Engineering, Rail Vehicles, Stockolm, 2008

[19] MICHÁLEK, T., ZELENKA, J.: Reduction of lateral forces between the railway vehicle and the track in small-radius curves by means of active elements, University of West Bohemia, 2011

[20] SIMPACK AG.: SIMPACK Documentation, 2013

[21] GHOSH, S.: Signals and Systems, Pearson Education, 2006

[22] JOHANNESSON, P., SPECKERT, M.: Guide to Load Analysis for Durability in Vehicle Engineering, Automotive Series, 2013

[23] LEE, Y-L., Fatigue Testing and Analysis, Theory and Practice, Elsevier, 2005

[24] ARIDURU, S.: Fatigue Life Calculation by Rainflow Cycle Counting Method, Thesis, Graduate School of Natural and Applied Sciences of Middle East Technical University, 2004

[25] NIJSSEN, R.P.L.: Fatigue Life Prediction and Strength Degradation of Wind Turbine Rotor Blade Composites, Delft University of Technology, 2006

[26] OLAGNON, M., GUÉDÉ, Z.: Rainflow fatigue analysis for loads with multimodal power spectral densities, Ifremer Centre de Brest, France, Marine Structures 21, 160-167, 2007

[27] HALPENNY, A.: A frequency domain approach for fatigue life estimation from Finite Element Analysis, International Conference on Damage Assessment of Structures, Dublin, 1999

[28] SIEMENS AG Transportation System: The COMBINO® three-section and five-section, low-floor articulated tramcar, Technical Information.

[29] SIEMENS AG Transportation System, First Class Bogies, The complete programme for high-quiality railway transportation.

[30] TALGO S.A.: URL http://www.talgo.com/index.php/en/rueda.php, October 2014

[31] RBC FRANCE: URL http://www.railway-technology.com/contractors/bogies/rbc/, October 2014

[32] HONDIUS, H.: Multigelenk-Straβenbahnen mit durchgehenden Achsen, Technik, Der Nahverkehr 1-2, 2005.

[33] MANESIS S. A., KOUSSOULAS N. T., DAVRAZOS G. N.: Off-Tracking elimination in Multi-Articulated Vehicles, University of Patras, Greece, 2005.

[34] DELLMANN T., ABDELFATTAH, B.: Multigelenkwagen vs. Einzelgelenkwagen – Strassenbahnkonzepte im Vergleich, Aachen, 2011.

A Appendix

Matlab function

A function has been created to obtain the so called Rainflow Matrix representation. The steps follow on the code to achieve this are shown in Figure B.1. First, the local maxima and minima of the load history are obtained. After that, the 4-point Algorithm is applied to these data, obtaining the closed cycles and the residual, recorded both in two different matrixes. The Rainflow Matrix is usually represented in a 30x30 format, therefore, the closed cycles data are then transformed to achieve this representation.

```
function totmaxmin(y)
%Initialization of variables
    n=length (y);
    i=1;
    j=2;
    maxmin(1)=y(1);
%Loop to save all the local maxima and minima of the load history.
    while i<(n-1)
        if (y(i+1)>y(i))&&(i<n)
            while y(i+1)>y(i) && i<(n-1)
                i=i+1;
            end
            if i==(n-1)
                maxmin(j)=y(i);
                maxmin(j+1)=y(i+1);
            else
                maxmin(j)=y(i);
                j=j+1;
            end
        elseif (y(i+1)<=y(i))&&(i<n)
           while y(i+1)<=y(i) && i<(n-1)
                i=i+1;
           end
           if i==(n-1)
                maxmin(j)=y(i);
                maxmin(j+1)=y(i+1);
           else
                maxmin(j)=y(i);
                j=j+1;
           end
        end
    end
%Loop to apply the Rainflow 4-Point Algorithm obtaining two matrixes:
the closed cycles and the residual.
    i=1;
    j=1;
    m=length(maxmin);
    while j<m-3
        s1=maxmin(j);
        s2=maxmin(j+1);
        s3=maxmin(j+2);
        s4=maxmin(j+3);
        if (min(s1,s4)<=min(s2,s3)) && (max(s2,s3)<=max(s1,s4))
            closed_cycles(i,1)=s2;
            closed_cycles(i,2)=s3;
```

```
            i=i+1;
            for k=0:(m-j-3)
                maxmin(j+1+k)=maxmin(j+3+k);
                k=k+1;
            end
            maxmin(m-1)=[];
            maxmin(m-1)=[];
            m=length(maxmin);
            j=0;
        end
        j=j+1;
    end
%Calculation of the Pseudo Damage Number
    d=0;
    for m=1:length(closed_cycles)
        d=d+(abs(closed_cycles(m,1)-closed_cycles(m,2)))^5;
    end
%Creation of the final Rainflow Matrix
%Rainflow Matrix Initialization
    for i=1:33
          for j=1:33
            matrix(i,j)=0;
           end
    end
%Tranformation of the closed cycles recorded to save them into a 1x30
matrix and graphical representation of it.
    maxim=max(max(closed_cycles));
    minim=min(min(closed_cycles));
    c=(maxim-minim)/31;
      for i=1:length(closed_cycles)
        k=1;
        m=1;
        while closed_cycles(i,1)>(minim+(k-1)*c)
            k=k+1;
        end
        while closed_cycles(i,2)>(minim+(m-1)*c)
            m=m+1;
        end
            matrix(k,m)=matrix(k,m)+1;
      end
%Representation of the Rainflo Matrix created
contourf(matrix)
%Change in the format of the grpah created. Legend, Title, Axis and Axis
Legend
colorbar
format short e
title(['Rainflow Matrix | d = ',sprintf('%0.3e',d),' kN^5 '])
set(gca,'XtickLabels',[minim+4*c, minim+9*c, minim+14*c, minim+19*c,
minim+24*c, minim+29*c]);
set(gca,'YtickLabels',[minim+4*c, minim+9*c, minim+14*c, minim+19*c,
minim+24*c, minim+29*c]);
xlabel('To')
ylabel('From')

 end
```

Figure B.1: MATLAB Function code

Example of Application

Taking a data example obtained from SIMPACK, its graphical representation in MATLAB (see Figure B.3) is done by the command shown in Figure B.2. To obtain the Rainflow Matrix of the load history under study, the command show in Figure B.4 should be written. Then, the Rainflow Matrix is obtained, see Figure B.5.

```
plot (SPCK_Result.Crv.x,SPCK_Result.Crv.y)
```

Figure B.2: command for the graphical representation of the data.

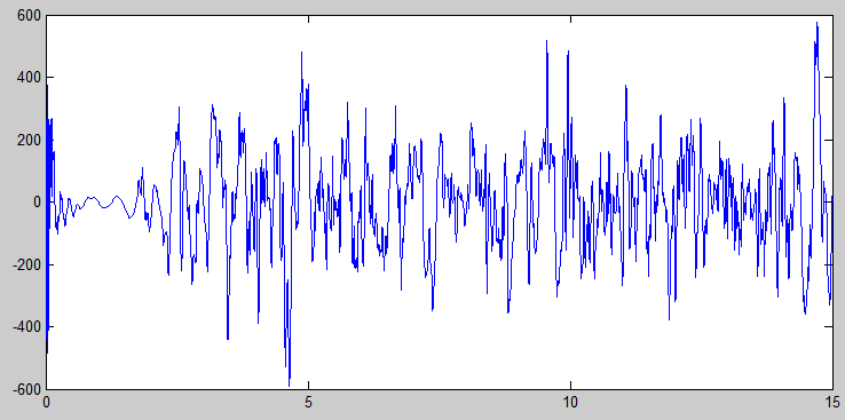

Figure B.3: graphical representation of the data.

```
totmaxmin(SPCK_Result.Crv.y)
```

Figure B.4: command to obtain the RFM of the load history obtained in SIMPACK.

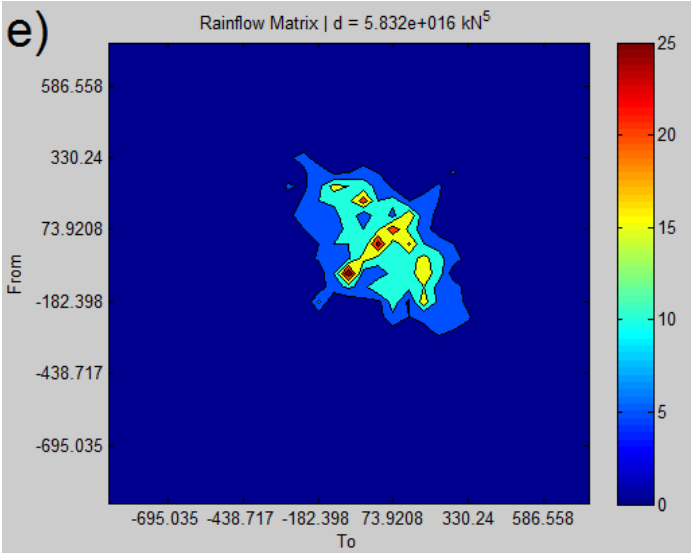

Figure B.5: RFM obtained of the load history under study.